



UNIVERSIDADE FEDERAL DO PARÁ  
INSTITUTO DE GEOCIÊNCIAS  
CURSO DE PÓS-GRADUAÇÃO EM GEOFÍSICA  
MASTER DEGREE DISSERTATION

**EXPERIMENTAL VERIFICATION OF HUDSON AND ESHELBY-  
CHENG'S EFFECTIVE CRACK THEORY**

JÉSSICA PENA HENRIQUES

Belém-Pará

2015

JÉSSICA PENA HENRIQUES

**EXPERIMENTAL VERIFICATION OF HUDSON AND ESHELBY-  
CHENG'S EFFECTIVE CRACK THEORY**

Dissertation submitted to the Postgraduate Program  
in Geophysics of the Universidade Federal do Pará  
for obtaining a Master's Degree in Geophysics.

Advisor: José Jadsom Sampaio de Figueiredo

Belém-Pará

2015

Dados Internacionais de Catalogação na Publicação (CIP)  
Biblioteca do Instituto de Geociências/SIBI/UFGA

---

Henriques, Jéssica Pena, 1992-

Experimental verification of Hudson and Eshelby-Cheng's effective crack theory / Jéssica Pena Henriques. – 2015  
59 f. : il. ; 29 cm

Inclui bibliografias

Orientador: José Jadsom Sampaio de Figueiredo  
Dissertação (Mestrado) – Universidade Federal do Pará,  
Instituto de Geociências, Pós-Graduação em Geofísica, Belém, 2015  
1. Geofísica. 2. Anisotropia. I. Título.

CDD 22. ed. 551

---

JÉSSICA PENA HENRIQUES

**EXPERIMENTAL VERIFICATION OF HUDSON AND ESHELBY-  
CHENG'S EFFECTIVE CRACK THEORY**

Dissertation submitted to the Postgraduate  
Program in Geophysics of the Universidade  
Federal do Pará for obtaining a Master's  
Degree in Geophysics.

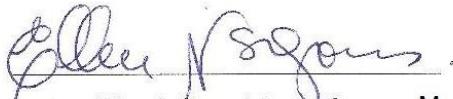
Approval date: 04/12/2015

Grade: BOM (8/10)

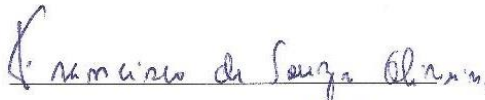
Committee Members:



Prof. José Jadsom Sampaio de Figueiredo – Advisor  
Doutor em Ciências e Engenharia do Petróleo.  
Universidade Federal do Pará



Profa. – Ellen de Nazaré Souza Gomes - Member  
Doutora em Geofísica  
Universidade Federal do Pará



Francisco de Souza Oliveira - Member  
Doutor em Geofísica  
Universidade Federal do Pará

## ACKNOWLEDGMENTS

I thank God and our holy mother for being there for me whenever I needed them.

To my mother for being my absolute everything, beyond my biggest example of person and love.

To my family, especially, my grandparents Luzia Sandim (*In memorian*) and Antenor Pena, aunt Zélia, uncle Edson e my sister from heart Rose and your family for support me.

To my advisor José Jadsom Sampaio de Figueiredo for invited me and believed in this work.

To my teachers Carolina Barros and Alberto Leandro.

To INCT-GP/CNPQ and PROPESP-UFGA by financial support. Also grateful to Profa. Ellen Gomes and Prof. Jesse Costa for providing support in the laboratory equipment's acquisition.

To Centro de Apoio à Pesquisa (CAPES) for financial support.

To my friends Carlos Eduardo and João Alves for support me since graduation.

To my friends Isadora Macedo and Léo Santos for support me in master's degree.

To students Ícaro Coutinho, Felipe Louzeiro and Mykel Sousa because it were essential in the construction of this work.

To all my friends.

To staff of CPGf for always help me.

To UFGA, CPGf and IG by the structure given to this work .

*“Acredite em si próprio e chegará um dia em que os outros não terão outra escolha senão acreditar com você”*

*(Cynthia Kersey)*

## RESUMO

A modelagem física em escala reduzida de meios fissurados/fraturados em laboratório tem servido como uma ótima alternativa para compreender o comportamento de meios anisotrópicos. Neste trabalho foram realizadas medidas ultrassônicas em amostras com baixas densidades e diferentes razões de aspecto de fissura. O objetivo principal se deu em investigar o comportamento dos parâmetros elásticos (velocidade das ondas, parâmetros de Thomsen  $\epsilon$  e  $\gamma$ ) e dos coeficientes do tensor de rigidez elástica para meios transversalmente isotrópicos. Comparar os resultados obtidos com as previsões feitas pelos modelos de Hudson (1981) e Eshelby-Cheng (1993) também foi investigado neste trabalho. Foram confeccionadas doze amostras com dois tipos de densidade de fissuras, 5 e 8%. As fissuras que possuem três razões de aspecto diferentes (0,133, 0,1778 e 0,2667) eram formadas por inclusões de borrachas em uma matriz isotrópica homogênea de resina. Além disso, uma matriz puramente isotrópica foi construída apenas por resina epóxi. Dentre todas as amostras, seis (três para cada densidade) possuem apenas um tipo de razão de aspecto (puras), enquanto outras seis (três para cada densidade) possuem três tipos de razões de aspectos diferentes (mistas). Entre as previsões dos modelos, o de Eshelby-Cheng (1993) mostra um melhor ajuste em relação aos resultados experimentais para as amostras puras (para as duas densidades de inclusões). No entanto, nenhum dos modelos prevê com mínima precisão a tendência para as amostras mistas.

Palavras-chave: Petrofísica. Meios anisotrópicos. Meios fissurados. Modelo de Hudson. Modelo de Eshelby-Cheng.

## ABSTRACT

Physical modeling of cracked / fractured media in downscaled laboratory experiments has served as a great alternative for understanding the anisotropic media behavior. In this work, it was performed ultrasonic measurements on samples with low crack densities and different aspect ratios. The main goal was to investigate the experimental behavior of elastic parameters, such as: waves velocities and Thomsen parameters  $\epsilon$  and  $\gamma$  and elastic stiffness coefficients for transverse isotropic media. Comparison of the results with the predictions made by the effective models of Hudson (1981) and Eshelby-Cheng (1993), it was also investigated in this work. Twelve samples were prepared with two types of cracks density, 5 and 8%. The cracks that have three different aspect ratios (0.133, 0.1778 and 0.2667) were formed by rubber inclusions in a homogeneous isotropic matrix resin. Moreover, an isotropic matrix sample was constructed by only epoxy resin. Among all samples, six (three for each density) have only one aspect ratio type (samples with single crack), while another six (three for each density) have three types of different aspect ratio (mixed samples). Among the predictions of the models, the Eshelby-Cheng (1993) shows a better fit in relation to the experimental results for samples with single crack (for the two densities of inclusions). However, none of the models predicts accurately with minimal tendency for the mixed samples.

Key words: Petrophysics. Anisotropic media. Cracked media. Hudson's model. Eshelby-Cheng's model.

## LIST OF ILLUSTRATIONS

Figure 2.1- (a) Photograph of the cracked samples with (b) 5% crack density and (b) 8% crack density and the reference sample SFC4 (uncracked). .....	20
Figure 2.2- Define of aspect ratio. ....	22
Figure 2.3- Picture of ultrasonic system used in this work.....	26
Figure 2.4- Device developed for (a) P-wave and (b) S-wave polarization rotation and velocity measurements. Sketch of experiment used for (c) P-wave and (d) S-wave seismogram records.....	26
Figure 2.5- (a) Waveforms for P-wave and S-wave transducers and (b) their corresponding frequency spectrum.....	28
Figure 3.1- P-wave seismograms as a function of change in p-wave polarization from $0^\circ$ (x direction) to $90^\circ$ (z direction) for sample SFC4 (isotropic). ....	31
Figure 3.2- Unfiltered P-waveforms as a function of change in P-wave polarization for $0^\circ$ (x direction) to $90^\circ$ (z direction) for all samples with crack density of 5%. ...	31
Figure 3.3- Unfiltered P-waveforms as a function of change in P-wave polarization for $0^\circ$ (x direction) to $90^\circ$ (z direction) for all samples with crack density of 8%. ...	32
Figure 3.4- Filtered P-waveforms as a function of change in P-wave polarization for $0^\circ$ (x direction) to $90^\circ$ (z direction) for all samples with crack density of 5%.....	32
Figure 3.5- Filtered P-waveforms as a function of change in P-wave polarization for $0^\circ$ (x direction) to $90^\circ$ (z direction) for all samples with crack density of 8%.....	33
Figure 3.6- S-wave seismograms as a function of change in polarization from $0^\circ$ to $180^\circ$ for propagation in the Y direction in the reference sample (SFC4).....	34
Figure 3.7- S-wave seismograms as a function of change in polarization from $0^\circ$ to $180^\circ$ for propagation in the Y direction in the samples with 5% crack density before filtering.....	35
Figure 3.8- S-wave seismograms as a function of change in polarization from $0^\circ$ to $180^\circ$ for propagation in the Y direction in the samples with 8% crack density before filtering.....	35
Figure 3.9- S-wave seismograms as a function of change in polarization from $0^\circ$ to $180^\circ$ for propagation in the Y direction in the samples with 5% crack density after filtering and with the indicate of S1 and S2.....	36
Figure 3.10- S-wave seismograms as a function of change in polarization from $0^\circ$ to $180^\circ$ for propagation in the Y direction in the samples with 8% crack density after filtering and with the indicate of S1 and S2.....	37
Figure 3.11- Constants of elastic stiffness tensor for 5% crack density. The green line show trends of Hudson's model with first correction, the red line trends of Hudson's model with second correction, the blue line trends of Eshelby-Cheng's model, the blue triangles are samples with single crack and red squares are mix cracks.....	38
Figure 3.12- Constants of elastic stiffness tensor for 8% crack density. The green line show trends of Hudson's model with first correction, the red line trends of	

Hudson's model with second correction, the blue line trends of Eshelby-Cheng's model, the blue triangles are samples with single crack and red squares are mix cracks.....	39
Figure 3.13- Thomsen's parameter of 5% crack density with samples and trends of Hudson (first correction in green line and second correction in red line) and Eshelby-Cheng models (in blue line).....	40
Figure 3.14- Thomsen's parameter of 8% crack density with samples and trends of Hudson (first correction in green line and second correction in red line) and Eshelby-Cheng models (in blue line).....	40
Figure 4.1- Ratio between $\lambda/x_c$ (wavelength/distance between cracks) for all twelve samples.....	42
Figure 4.2- Ratio between $\lambda/d_c$ (wavelength/diameter of cracks) for all twelve samples.....	42
Figure 4.3- Thomsen's parameters for samples with mix cracks of 5% crack density with Voigt-Reuss average. The mix anisotropic values fits well between the lower (Reuss) upper (Voigt) bounds.....	46
Figure 4.4- Thomsen's parameters for samples with mix cracks of 8% crack density with Voigt-Reuss average. The mix anisotropic values did not between the lower (Reuss) upper (Voigt) bounds.....	46
Figure 4.5- Thomsen's parameters (predicted by Eshelby-Cheng's (1993) model) for samples with mix cracks of 5% crack density with Voigt-Reuss average. The mix anisotropic values fits well between the lower (Reuss) upper (Voigt) bounds.....	47
Figure 4.6- Thomsen's parameters (predicted by Eshelby-Cheng's (1993) model) for samples with mix cracks of 8% crack density with Voigt-Reuss average. The mix anisotropic values fits well between the lower (Reuss) upper (Voigt) bounds.....	48

## LIST OF SYMBOLS

$C_{ij}^{eff}$	Elastic stiffness tensor	$e_c$	Crack density
$\sigma$	Stress	$\alpha$	Aspect ratio
$\epsilon$	Strain	$N_i$	Number of cracks
$C_{ij}$	Constants of elastic stiffness tensor	$C_{\%}$	Percentage of cracks
$V_p$	P wave velocity	$V_c$	Volume of crack
$V_{p_x}$	P wave velocity faster	$b_t$	Thickness of crack
$V_{p_z}$	P wave velocity slower	$\alpha_{pure}$	Aspect ratio of samples with single crack
$V_s$	S wave velocity	$\alpha_{mix}$	Aspect ratio of samples with mix cracks
$V_{s_1}$	S wave velocity faster	$d_c$	Crack diameter
$V_{s_2}$	S wave velocity slower	$r_c$	Crack radius
$\rho$	Density	$l_c$	Distance of cracks.
$\epsilon$	Thomsen's parameter of P wave		
$\gamma$	Thomsen's parameter of S wave		

## LIST OF TABLES

Table 2.1- Types of cracks and aspect ratios.....	21
Table 2.2- Physical parameters of uncracked and cracked samples. Precision of length measurements is about 0.1 cm. ....	23
Table 2.3- Description of cracks the samples.....	24
Table 3.1- Compressional wave velocities (for X and Z directions) and anisotropic parameter $\varepsilon$ calculated according to equation (7).....	33
Table 3.2- Shear wave velocities (for Y direction) and anisotropic parameter $\gamma$ calculated according to equation (8).....	37
Table 4.1- Groups in which the samples are divided.....	43

## SUMMARY

<b>CHAPTER 1</b> .....	<b>13</b>
<b>1.1 Theoretical Background</b> .....	<b>15</b>
<b>1.2 Crack models description</b> .....	<b>15</b>
<b>1.3 Effective crack models description</b> .....	<b>17</b>
<b>CHAPTER 2</b> .....	<b>19</b>
<b>2.1 Experimental procedure</b> .....	<b>19</b>
<b>2.2 Sample preparation</b> .....	<b>19</b>
<b>2.3 Ultrasonic measurements</b> .....	<b>24</b>
<b>CHAPTER 3</b> .....	<b>29</b>
<b>3.1 Experimental results</b> .....	<b>29</b>
<b>3.2 Compressional wave (P) velocities</b> .....	<b>29</b>
<b>3.3 Shear wave (S) velocities</b> .....	<b>34</b>
<b>3.4 Elastic stiffness tensor components</b> .....	<b>37</b>
<b>3.5 Thomsen's parameters</b> .....	<b>39</b>
<b>CHAPTER 4</b> .....	<b>41</b>
<b>4.1. Discussions</b> .....	<b>41</b>
4.1.1. Compressional (P) and shear (S) velocities .....	43
4.1.2. Coefficients of elastic stiffness tensor.....	44
4.1.3. Thomsen's parameters.....	44
<b>CHAPTER 5</b> .....	<b>49</b>
<b>5.1 Conclusions</b> .....	<b>49</b>
<b>REFERENCES</b> .....	<b>51</b>
<b>APPENDICES</b> .....	<b>53</b>
<b>APPENDIX A</b> .....	<b>54</b>
<b>APPENDIX A.1- EFFECTIVE MODULI BY HUDSON</b> .....	<b>54</b>
<b>APPENDIX A.2 - EFFECTIVE MODULI BY CHENG</b> .....	<b>56</b>

## CHAPTER 1

In the subsurface of the earth, in addition to bedding of rock layers with thicknesses less than the length of the seismic wave, the anisotropic behavior of a medium may also be induced by cracks or fractures preferentially oriented. This type of analysis of the presence of cracks and fractures in the subsurface has aroused great interest in both the oil industry and academy. In the case of fractured reservoirs, to understand of the crack density and aspect ratio is essential to optimize the exploitation and oil production (NELSON, 2001). Regions that have fractured preferred orientation induce variations in wave velocities (P and S) dependent on the direction of propagation. Thus, elastic seismic waves can be used as a tool to determine these orientations or crack densities (SAYERS,2007). Due of the need to better understand fractured reservoirs, investigations related to anisotropic media have received increasing attention from the oil industry (WILD, 2011).

Because numerical dispersion problems that can be found in the modeling of cracks and fractures (COATES;SCHOENBERG, 1995; ZHANG, 2005), usually is done the replacement of the cracks and fractures by an effective medium in which the individual effect of fractures or cracks can not be performed (SAENGER; SHAPIRO, 2002). Using physical modeling the problem of numerical ambiguous answer is not found in order that cracks and fractures can be physically simulated by materials having a very low shear modulus (e.g. rubber) with different physical characteristics (ASSAD et al., 1992, 1996).

Unlike to the numerical modeling, physical modeling of the seismic or ultrasonic data is a more accurate simulation method to a seismic investigation. First, a physical model is performed in order to simulate a geology desired through a downscale procedure, but need careful physical mounting structure and geological bodies using synthetic materials whose elastic properties are previously known. Then simulate the seismic experiment with the issue of acoustic high-frequency signals (upscale of source frequency), such as ultrasound or ultrasonic lasers aimed simulate the wave field scattered.

Anisotropic modeling through experimentally scaled physical modeling is alternatives for understand how is the behavior of cracked medium. This alternative is valid

because in laboratory measurements are possible to modeling conditions present in the field (FIGUEIREDO et al., 2013). Rathore et al., (1995) measured P- and S- in manufactures dry samples made of sand-epoxy matrix and compare with Hudson's and Thomsen's models. Assad (1992, 1996) constructed samples with rubber penny-shaped inclusions with different crack densities in an epoxy resin matrix. In this work, comparisons between the relations of crack density versus  $\gamma$  Thomsen (1986) parameter was performed related to the predictions by Hudson (1981)'s model. The series of papers of Figueiredo et al., (2012, 2013) and Santos et al. (2015) show physical-modeling experiment with an artificially anisotropic cracked model made with a matrix of epoxy resin with inclusions of rubber. Figueiredo et al., (2012) and Santos et al. (2015) models that had different fractures orientations, P- and S- waves were measured and Thomsen's parameters were correlated with the fracture orientation. In the second the synthetic samples have just one alignment of cracks, but different crack density and aspect ratio in order to investigate the effect of source frequency on the elastic parameters and shear wave attenuation of the medium.

In general, effective theoretical models for cracked anisotropic medium to long-wavelength theories where the response of medium to be homogeneous (Hudson and Liu, 1999). Eshelby (1957) proposed a model for determination elastic field and the problems that involved for isotropic matrix with ellipsoidal inclusion. After this paper, Hudson (1981) proposed an effective modulus in an elastic solid with thin, penny-shaped ellipsoidal cracks or inclusions for low crack density. Lastly, Cheng (1993), based on the Eshelby (1957) work, proposed too an effective modulus in an elastic solid with ellipsoidal inclusion, that resembles with Hudson (1981), but with different considerations. This is a generalization of Hudson (1981) theory in view of the Eshelby-Cheng model (1993) there is no limitation about crack aspect ratio.

In this work were constructed one uncracked sample, as reference, and twelve cracked samples. The crack or inclusions were simulated physically by of penny-shaped rubber inclusions. Three different aspect ratio crack were used in the cracked samples. The samples are divided in two groups of crack density: 5 and 8%. The two groups were divided e two sub groups that have same density but different aspect ratio cracks. These samples were called by single (single aspect ratio cracks) and mix (sample with different aspect-ratio crack). The P- and S- wave records were measured as function of the angle of incidence, and then were calculated the velocities, stiffness

coefficients of these two Thomsen's parameters ( $\varepsilon$  and  $\gamma$ ). After this, comparisons of our results with the predictions made by the effective models of Hudson (1981) and Eshelby-Cheng (1993), it was performed.

Is important to highlight that this work has format of paper, for this reason the work has a smaller the usual structure of master thesis. However, this dissertation is divided in five chapters. The first describes the crack models (anisotropic media) and effective crack models of Hudson (1981) and Eshelby-Cheng (1993). The second explains the process of samples preparation and ultrasonic experimental setup. The experimental results are shown in third chapter. And the last two chapters show the discussions and conclusions about experimental results in comparison with theoretical curves of Hudson (1981) and Eshelby-Cheng's (1993) models.

## 1.1 Theoretical Background

This chapter aim to show elastic stiffness coefficients as well as the anisotropic parameters associated to the P- and S-waves propagation. Besides, presents the theoretical background necessary to understand the theoretical models for cracked samples of Hudson (1981) and Eshelby-Cheng (1993), which will be used to compare with our experimental results.

## 1.2 Crack models description

Any anisotropic medium can be represented mathematically by the elastic stiffness tensor ( $C_{ij}^{eff}$ ) that is a linearly proportional between the stress applied ( $\sigma$ ) on the medium and their strain ( $\epsilon$ ). In simplified notation, the Hooke's equation is given by:

$$\sigma_i = C_{ij}^{eff} \epsilon_j \quad (1)$$

Theoretical models have their mathematical description of the medium trough the effective moduli given by the matrix  $C_{ij}^{eff}$ . In a transversely isotropic (TI) medium, the matrix has five independent constants. In matrix form, the  $C_{ij}^{eff}$  can be representing by:

$$C_{ij}^{eff} = \begin{pmatrix} C_{11} & C_{12} & C_{13} & 0 & 0 & 0 \\ C_{13} & C_{33} & C_{33} - 2C_{44} & 0 & 0 & 0 \\ C_{13} & C_{33} - 2C_{44} & C_{33} & 0 & 0 & 0 \\ 0 & 0 & 0 & C_{44} & 0 & 0 \\ 0 & 0 & 0 & 0 & C_{66} & 0 \\ 0 & 0 & 0 & 0 & 0 & C_{66} \end{pmatrix} \quad (2)$$

In anisotropic media it is possible to observe three different modes of wave propagation: quasi-longitudinal, quasi-shear, and pure shear. The first type is related to the P-wave, in other words, related to P velocity ( $V_p$ ). It is important to know that  $V_p$  can change with the angle of incidence of the wave, because, in anisotropic medium, when the compressional wave propagates perpendicular to the cracks distribution, the  $V_p$  is slower than when cracks are parallel. The last two modes of wave propagation are related to S-wave. In this case, the particle motions are perpendicular to the direction of propagation. The S-wave modes are related to the quasi- and pure-shear wave. Both have perpendicular wave-vibration between them. These two modes are denominated by:  $V_{s1}$  and  $V_{s2}$ . Which  $V_{s1}$  is parallel to crack plane and  $V_{s2}$  is perpendicular to the crack plane. Consequently  $V_{s1}$  is faster than  $V_{s2}$ .

The dependence between velocities and the constants of elastic stiffness tensor, is given by:

$$C_{11} = V_p^2(90^\circ)\rho \quad (3)$$

$$C_{33} = V_p^2(0^\circ)\rho \quad (4)$$

$$C_{66} = V_{sh}^2(90^\circ)\rho \quad (5)$$

$$C_{44} = V_{sv}^2(90^\circ)\rho \quad (6)$$

where  $\rho$  is the medium density,  $V_{SH}=V_{s1}$  and  $V_{SV}=V_{s2}$ .

It is well established that Thomsen parameters  $\varepsilon$  and  $\gamma$ , describes the influence of the medium anisotropy on P- and S-wave propagations (Thomsen, 1986). The parameter  $\varepsilon$  is related to the velocities of P-wave propagation parallel ( $V_p(90^\circ)$ ) and perpendicular ( $V_p(0^\circ)$ ) to the fracture plane. While parameter  $\gamma$ , is related to the

velocities of the orthogonal shear-waves polarizations, S1 and S2. In this work, we are using the same notation for  $\varepsilon$  and  $\gamma$  as described in Thomsen (1986),

$$\varepsilon = \frac{C_{11} - C_{33}}{2C_{33}} \quad (7)$$

$$\gamma = \frac{C_{66} - C_{44}}{2C_{44}} \quad (8)$$

### 1.3 Effective crack models description

Two theoretical effective models to represent cracked media were suggested by Hudson (1981) and Eshelby-Cheng (1993). The first relies on cracked model represented by a host isotropic matrix filled by aligned penny-shaped ellipsoidal cracks with normal axes along of Z direction. The second one relies on theoretical crack model suggested by Cheng (1993), which was modified from Eshelby (1957) static solutions.

The Hudson (1981) model is based on scattering-theory analysis of the mean wavefield in a solid matrix filled by crack with small aspect ratio. The format of crack should assume a penny-shaped ellipsoidal inclusion. The effective moduli  $C_{ij}^{eff}$  for Hudson (1981) cracked model are given as

$$C_{ij}^{eff} = C_{ij}^0 + C_{ij}^1 + C_{ij}^2 \quad (9)$$

where  $C_{ij}^0$  is the isotropic elastic coefficients (host material), and  $C_{ij}^1$ ,  $C_{ij}^2$ , are the first and second correction of elastic moduli, respectively (see Appendix A to see the all Hudson's (1981) model description parameters). Hudson's model has second-order expansion that, besides is not uniformly converging series, predicts increasing moduli with crack density beyond the formal limit (Cheng, 1993). Despite this, in this work, were used the first and second-order correction.

The other effective theory investigated in this work was the Eshelby-Cheng (1993) model. The effective moduli  $C^{eff}$  for a rock containing fluid-filled ellipsoidal cracks are given as

$$C_{ij}^{eff} = C_{ij}^0 - \phi C_{ij}^1 \quad (10)$$

where  $\phi$  is the porosity and  $C_{ij}^1$  the first corrections due crack inclusions (see Appendix A to see the all Eshelby-Cheng (1993) model description parameters).

For all these models assumes an isotropic, homogeneous, elastic background matrix and an idealized ellipsoidal crack shape and without connectivity between cracks, this is meaning no flow. Both models only support crack density lower than 10 %. All samples constructed in this work, attend this supposition. The principal difference between Hudson's and Cheng's moduli is the first is extremely connected with a very small aspect ratio while Cheng's developed for arbitrary aspect ratio.

## CHAPTER 2

### 2.1 Experimental procedure

This chapter presents the experimental procedure for construction as well as the ultrasonic measurements in the cracked and uncracked synthetic samples. The main goal of these sample constructions is to reproduce in controlled conditions, anisotropic media to understand and verify the viability the use of effective anisotropic media theories such as Hudson (1981) and Eshelby-Cheng (1993).

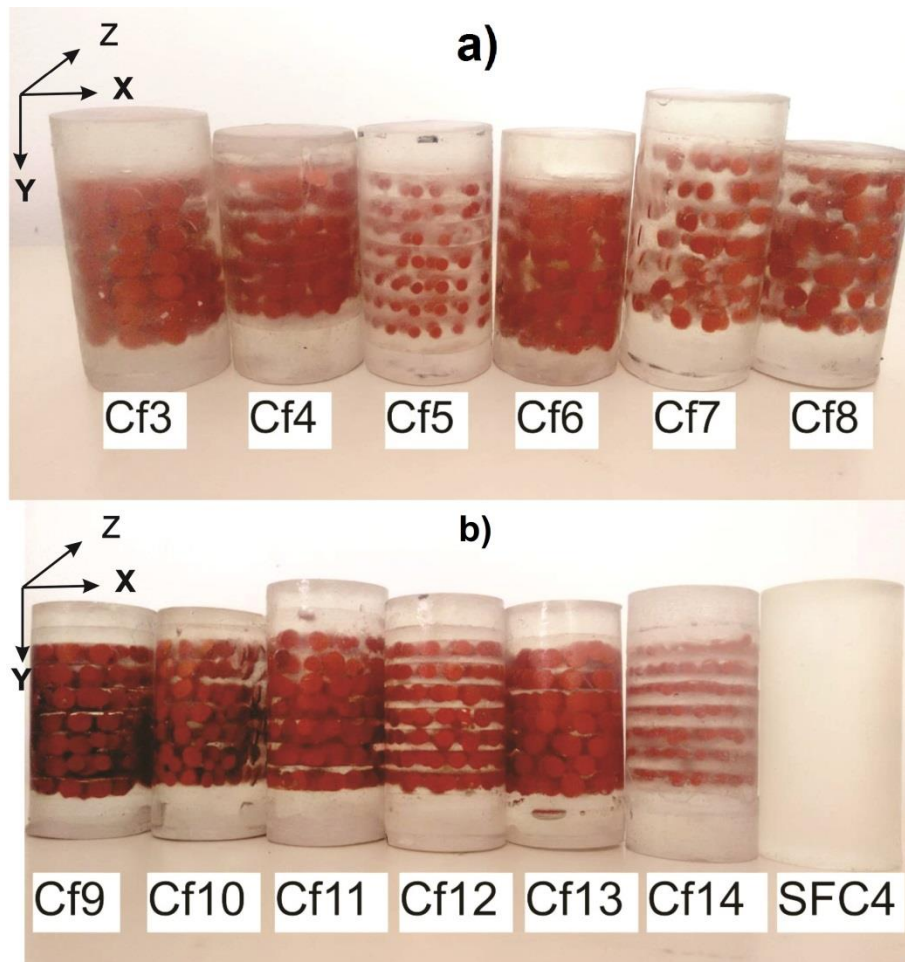
The construction of the cracked samples as well as the ultrasonic measurements was carried out at the Laboratory of Petrophysics and Rock Physics—Dr. Om Prakash Verma (LPRP) at the Federal University of Pará, Brazil. Under controlled conditions, it was constructed twelve cracked samples, divided in two groups of six samples. The first group, the crack density was of the 5% while the second, the crack density was of the 8%. In both of groups, cracks in the sample had different aspect ratio. An isotropic uncracked sample (SFC4) was constructed for reference. Pictures of all samples are shown in Figure 2.1.

### 2.2 Sample preparation

The uncracked sample (SFC4) consists of a single cast of epoxy resin. Samples CF3 to CF14 contain cracks aligned along the  $Y$  and  $X$  directions, respectively. In the samples of CF3 to CF8 has 5% of crack density and in the samples of CF9 to CF14 have 8% of crack density. All cracked samples were constituted one layer at a time, alternating with the introduction of rubber cracks. To reduce possible boundary effects to a minimum, the time interval between the creations of separate layers was kept as short as possible. The constant layer thickness (0.7 cm), it was ensured by using the same volume of epoxy resin poured for each layer. Each cracked sample has 7 layers. The solid rubber material used to simulate the cracks in all samples was silicone rubber. The compressional wave-velocity ratio was around 1.89 between solid epoxy and silicone rubber. Note that these values are only rough estimates, because the  $S$ -wave velocity in rubber was difficult to determine due to the low shear modulus of this material. The physical parameters of the included rubber cracks in each sample are

displayed in Table 2.1. All the cracks used in these samples have same thickness (crack aperture) of 0.08 mm.

Figure 2.1- (a) Photograph of the cracked samples with (b) 5% crack density and (b) 8% crack density and the reference sample SFC4 (uncracked).



Source: From author.

As mentioned in the previous chapter, the additional contributions of this work, beyond comparing theoretical predictions by a different approach (Hudson, 1981; Eshelby-Cheng, 1993) with experimental results, is verifying how the single and mixed crack's aspect-ratio distribution effects in the P and S-wave response. For this proposal, the samples CF4 to CF8 and CF9 to CF11 had cracks with mixed aspect-ratio.

It is worthy to mention, that all crack samples, contain oriented cracks with random distribution in the layers. Consequently, this preferential orientation leads to simulation of transversely isotropic medium. The HTI media is viewed from above of XZ plane and VTI when viewed from above of XY plane (see Figure 2.1).

Table 2.1- Types of cracks and aspect ratios.

Crack type	Crack diameter ( $d_c$ ) (mm)	Thickness ( $h_t$ ) (mm)	Aspect ratio ( $\alpha$ )
1	0.6	0.08	0.1333
2	0.45	0.08	0.1778
3	0.3	0.08	0.2667

Source: From author.

It was estimated the sample crack density ( $e_c$ ) for single and mix crack diameter in each cracked sample according to the modified Hudson (1981) formula. For cracked sample with single diameter, the crack density parameter is given by,

$$e_c = \frac{N\pi r^2 h_t}{V} \quad (11)$$

where  $N$  is total number of inclusions,  $r$  is their radius,  $h_t$  is the inclusion's thickness (crack aperture) and, finally,  $V$  is the volume of the cracked region for each sample.

In the case of crack density ( $e_c$ ) estimation for cracked samples with mix aspect ratio, it was developed for this work an adaption of equation (11) for more than one aspect ratio given by

$$e_c = \frac{\sum_{i=1}^3 NC_{\%i} Vc_i}{Vm} \quad (12)$$

where the crack volume is given by,

$$Vc = \pi r_c^2 h_t \quad (13)$$

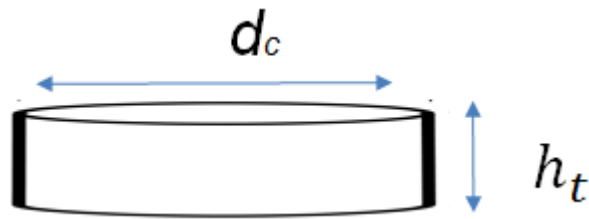
and the volume of crack regions is,

$$Vm = \pi r^2 h \quad (14)$$

where  $N$ ,  $C_{\%}$  and  $Vc$  are the number of inclusions, the percentage of each crack aspect-ratio and the volume of each cracks with different radius ( $\frac{d_c}{2} = r_c$ ) with the same thickness ( $h_t$ ), respectively.

Aspect ratio may be defined as a geometric feature of the fissure or crack like can see in Figure 2.2 and equation 15.

Figure 2.2- Define of aspect ratio.



Source: From author.

The aspect ratio ( $\alpha_{single}$ ) of the samples with just one type of crack (single aspect ratio samples) was calculated by,

$$\alpha_{single} = \frac{h_t}{d_c} \quad (15)$$

For samples with three types of cracks (mix diameter) the aspect ratio ( $\alpha_{mix}$ ) was calculated by

$$\alpha_{mix} = \sum_{i=1}^3 \alpha_i C_{\%i} \quad (16)$$

where  $C_{\%i}$  is the concentration of type of crack diameter.

The physical and geometrical parameters of the included rubber cracks in each sample are displayed in Table 2.2 and Table 2.3.

Table 2.2- Physical parameters of uncracked and cracked samples. Precision of length measurements is about 0.1 cm.

Sample	Length (Y)	Diameter (Z)	Density
Names	(cm)	(cm)	(kg/m <sup>3</sup> )
SFC4	7.551± 0.02	3.598± 0.02	1239.5
CF3	6.81± 0.02	3.707± 0.02	1233.7
CF4	6.399± 0.02	3.705± 0.02	1208.5
CF5	6.556± 0.02	3.616± 0.02	1307.3
CF6	6.538± 0.02	3.646± 0.02	1216.7
CF7	7.518± 0.02	3.627± 0.02	1236.8
CF8	6.579± 0.02	3.742± 0.02	1182.6
CF9	7.008± 0.02	3.656± 0.02	1254.1
CF10	6.906± 0.02	3.7± 0.02	1208.9
CF11	7.742± 0.02	3.649± 0.02	1256.6
CF12	7.282± 0.02	3.643± 0.02	1233.3
CF13	7.25± 0.02	3.699± 0.02	1214.4
CF14	7.561± 0.02	3.699± 0.02	1219.2

Source: From author

Table 2.3- Description of cracks the samples.

Sample Names	Crack density ( $e_c$ )	Type of crack			Aspect ratio	Number of cracks for layer		
		1	2	3		Crack 1	Crack 2	Crack 3
SFC4	0%	0	0	0	-	0	0	0
CF3	5%	100%	0%	0%	0.1333	14	0	0
CF4	5%	0%	100%	0%	0.1778	0	19	0
CF5	5%	0%	0%	100%	0.2667	0	0	24
CF6	5%	50%	30%	20%	0.1733	10	6	4
CF7	5%	40%	40%	20%	0.1778	8	8	4
CF8	5%	30%	50%	20%	0.1822	7	11	5
CF9	8%	50%	30%	20%	0.1733	16	10	6
CF10	8%	40%	40%	20%	0.1778	14	14	7
CF11	8%	30%	50%	20%	0.1822	11	18	7
CF12	8%	0%	100%	0%	0.1778	0	30	0
CF13	8%	100%	0%	0%	0.1333	23	0	0
CF14	8%	0%	0%	100%	0.2667	0	0	46

Source: From author

## 2.3 Ultrasonic measurements

The ultrasonic measurements were performed using the Ultrasonic Research System at LPRF with the pulse transmission technique. The sampling rate per channel for all measures of P and S-wave records was 0.1  $\mu$ s. Figure 2.3 shows a picture of ultrasonic system used in this work. The system is formed by: a pulse-receiver 5072PR and pre-amplifier 5660B from Olympus, a USB oscilloscope of 50 MHz from Handscope and P and S-wave transducers of 1 MHz also from Olympus.

Figure 2.4 shows the device developed for recording P-wave and S-wave seismograms, with rotating polarization for both. The source and receiver transducers were arranged on opposing sides of the samples, separated by the length of the sample measured (Table 2.2). To ensure the propagation of wave was in the desired region of the samples, the transducers were placed at the center of either side. This was made for both wave modes of propagation.

In case of P-wave recording, the initial compressional wave polarization was perpendicular to the cracks plane, in the other words, in the XY plane (see Figure

2.4 a) and b), from there were made measurements every  $10^\circ$  at a time until the sample is  $90^\circ$  (polarization was perpendicular to the cracks plane). In total, ten traces of P-wave were recorded in each sample.

For shear wave, the initial polarization was parallel to the cracks, in XY plane (see Figure 2.4 c and d), were made measures every  $15^\circ$  at a time until polarization was again parallel, so  $180^\circ$ . Thirteen traces of S wave were recorded in each sample. The polarization of  $0^\circ$  and  $180^\circ$  correspond to the fast S-wave ( $S_1$ ) and  $90^\circ$  corresponds to the slow S-wave ( $S_2$ ).

To estimate the P-wave velocities were used the relation given as

$$V_p = \frac{L_p}{t_p - \Delta t_{delay}^p} \quad (17)$$

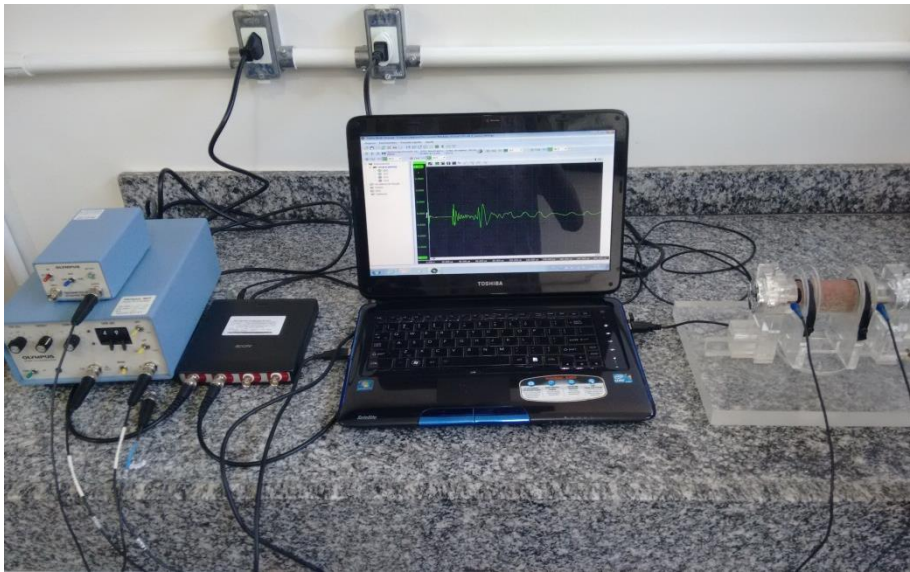
where  $L_p$  is the distance of P-wave propagation,  $t_p$  is the transmission travel time of P-wave and  $\Delta t_{delay}^p$  is the delay time of P-wave transducer. To S-wave velocities, the equation is similar to P-wave. They are given by

$$V_{S_1} = \frac{L_s}{t_{s1} - \Delta t_{delay}^s} \quad (18)$$

$$V_{S_2} = \frac{L_s}{t_{s2} - \Delta t_{delay}^s} \quad (19)$$

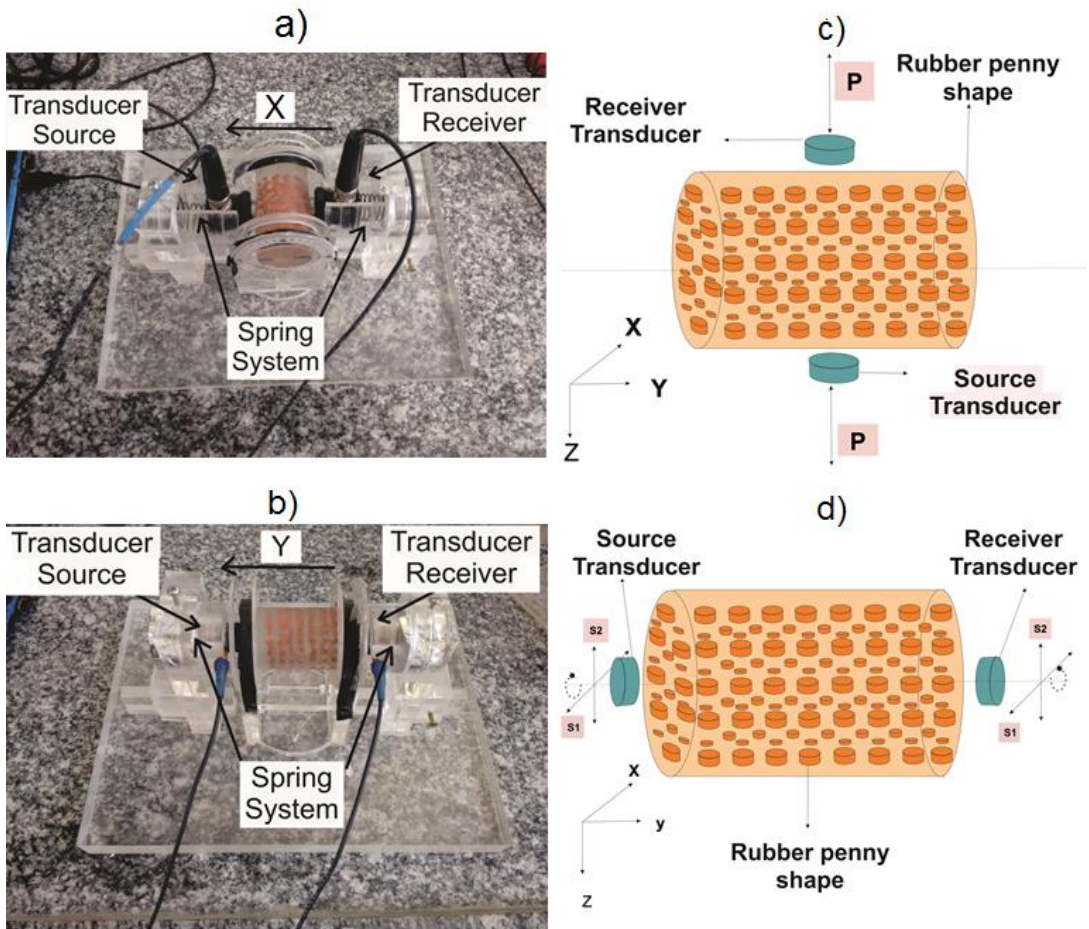
where  $L_s$  is the distance of S-wave propagation,  $t_{s1}$  and  $t_{s2}$  is the transmission travel time of S-wave propagation (fast and slower modes) and  $\Delta t_{delay}^s$  is the delay time of S-wave transducer.

Figure 2.3- Picture of ultrasonic system used in this work.



Source: From author.

Figure 2.4- Device developed for (a) P-wave and (b) S-wave polarization rotation and velocity measurements. Sketch of experiment used for (c) P-wave and (d) S-wave seismogram records.



Source: From author.

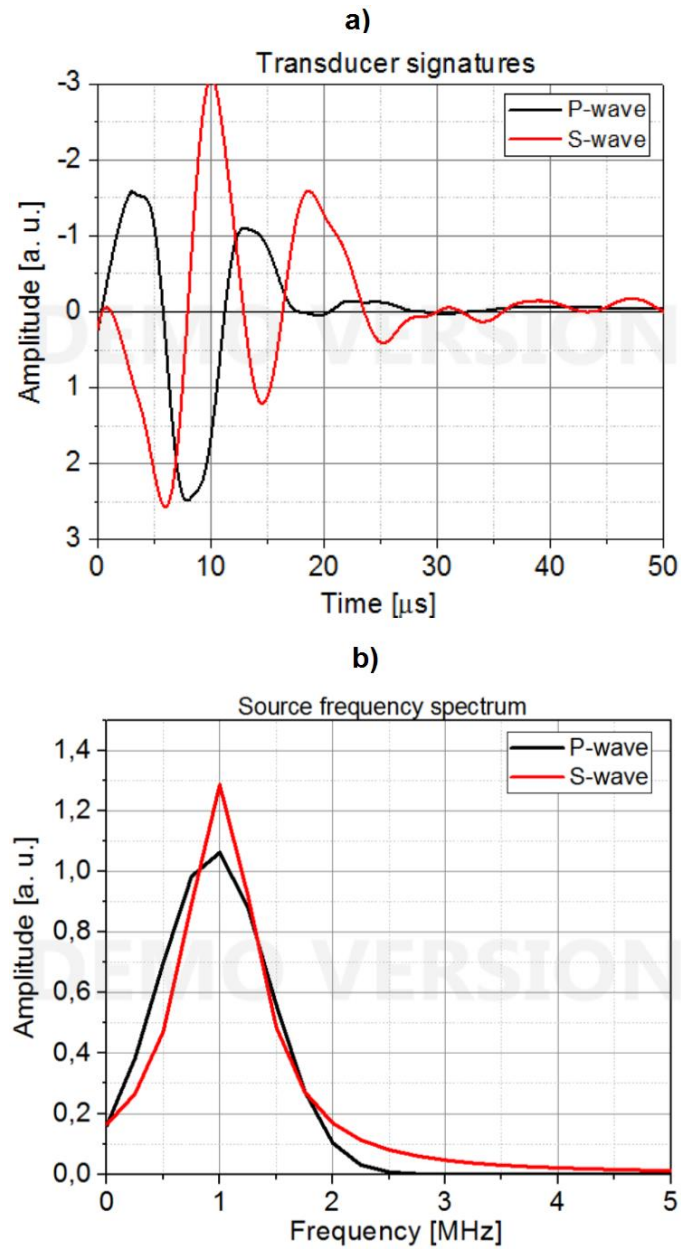
In order to ensure of the reproducibility of the ultrasonic recordings for all samples, it was preserved the same physical condition of the complete electronic apparatus. Furthermore, a holder with spring attached guaranteed the same coupling between transducer and samples (see Figure 2.4) and a very slim layer of natural honey was placed at the surface of the samples to establish good contact between transducer and samples too.

The domination frequency of the transducers P and S, as can be seen in Figure 2.5 a), is around 1 MHz and source wavelet pulse is the signature observed in Figure 2.5 b). More information about these transducers can be found at the website of the manufacturer<sup>1</sup>.

---

<sup>1</sup> Through: [www.olympus-ims.com/en/ultrasonic-transducers](http://www.olympus-ims.com/en/ultrasonic-transducers)

Figure 2.5- (a) Waveforms for P-wave and S-wave transducers and (b) their corresponding frequency spectrum.



Source: From author.

## CHAPTER 3

In this chapter, it is presented the experimental results for P-wave and S-wave velocities in twelve cracked samples and one uncracked sample. It also includes the comparison of the measured stiffness coefficients and anisotropic parameters with theoretical prediction by effective elastic coefficients for transversally isotropic media (TI), based on the theories of Hudson (1981) and Eshelby-Cheng (1993).

### 3.1 Experimental results

The results of ultrasonic measures are the time travel of waves. With this time travel, the first arrive was select and of this time was subtracted the time delay of P and S wave, that is  $1.03 \mu s$  and  $0.14 \mu s$ , respectively. With the information of lengths presents in Table 2.1 the velocities were calculated using equation (17), (18) and (19). For calculate the constants of elastic stiffness tensor have just use the information of Table 2.1 and the velocities in equations (3) to (6). Similar, Thomsen's parameter can be determined by the equations (7) and (8) after the determinations of constants of elastic stiffness tensor. It was calculated: P and S wave velocities, elastic stiffness tensor constants ( $C_{11}$ ,  $C_{33}$ ,  $C_{44}$  and  $C_{66}$ ) and the Thomsen's parameters ( $\epsilon$  and  $\gamma$ ) for all cracked samples considering the possible errors due to measurements of length (error margin of 0.02 cm) and time travel (error margin of  $0.02 \mu s$ )

### 3.2 Compressional wave (P) velocities

The analysis of this work it is started with the transmission seismograms for the reference sample (SFC4). The error margin of values of P-wave velocity is ranging from  $\pm 22.53$  m/s to  $\pm 27.72$  m/s and for S-wave is from  $\pm 7.07$  m/s to  $\pm 13.68$  m/s. The compressional wave can travel in any medium (including fluids like air, or, in the case of this work, rubber) unlike of shear wave. For this reason the anisotropy can be noticed easily with S-wave, because the contrast between the velocities in the background and inside the fissure is large.

Figure 3.1 shows ten compressional waveforms, each recorded with a (source-

receiver) pair of P-wave transducers on opposite sides of the model with initial polarization along of X axis ( $0^\circ$ ) and final polarization along of Z axis ( $90^\circ$ ). In other words, they represent the acquisition at 10 measurement points in the isotropic medium (SFC4). As expected, the seismograms recorded in the reference model show uniform first arrivals for all rotations of the polarization angle

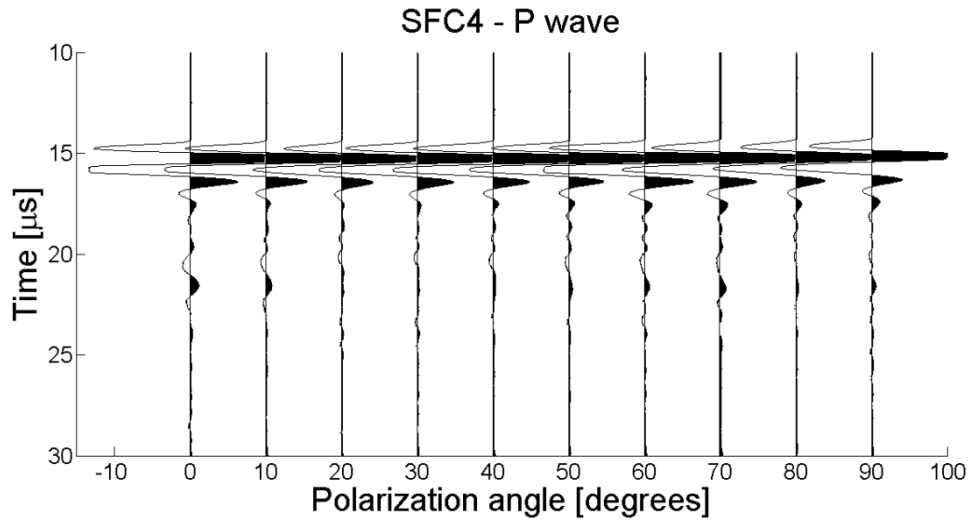
Figure 3.2 and Figure 3.3 shows the P-wave records in the six cracked samples of 5% and 8% of crack density, respectively, without filter. They represent the acquisition at the ten measurement points in the cracked sample, for propagation along the Z Figure 2.4 (c) and X Figure 2.4 (d) axes.

To better identify two separate peaks, we applied in most samples a band-pass filter of 200–400–600–800 kHz. The result obtained as the difference between the original and filtered seismograms, is shown in Figure 3.4.

Using the picked of first-arrival times of the bigger waveforms of depicted in Figure 3.4 and Figure 3.5 together with the propagation lengths in the Z and X directions in the cracked model (see Table 2.2), were determined the P-wave velocities ( $V_{px}(0^\circ)$  and  $V_{pz}(90^\circ)$ ) for propagation along these directions. Table 3.1 shows these velocities for the isotropic and cracked samples. Observe that the velocities  $V_{pz}$  e  $V_{px}$  are almost the same for samples CF5 e CF14 (samples with high cracked aspect-ratio). On the other hand,  $V_{pz}$  are significantly distinct of  $V_{px}$  for sample CF3 and CF13 (sample with low cracked aspect-ratio).

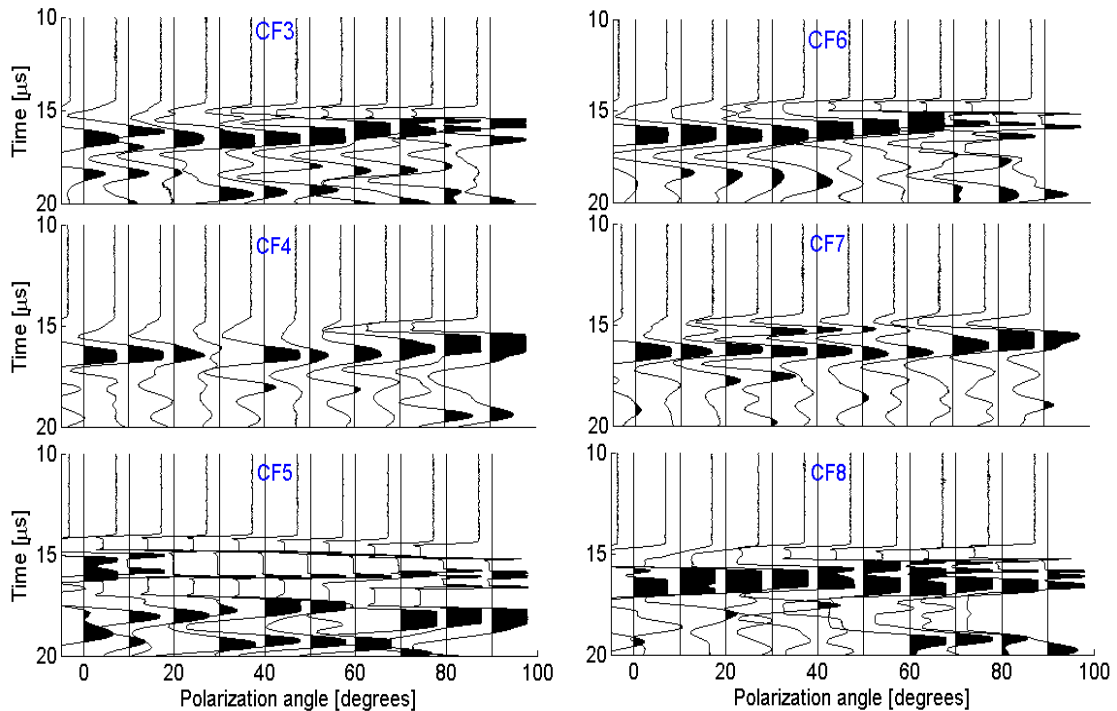
As an auxiliary parameter to describe the crack distribution using the P-wave velocity, was used the Thomsen (1986) parameter  $\epsilon$  (see equation (7)) derived directly from the orthogonal elements of the stiffness matrix ( $C_{ij}$ ) associated with the P-wave velocities ( $V_{px}$  and  $V_{pz}$ ). Table 3.1 shows the values of this parameter for the uncracked and cracked samples. It can be observed, that  $\epsilon$  has low values 5% crack density sample and low aspect-ratio inclusion, the values increases for increase of density (for 8% crack density sample) and in the case of low aspect-ratio inclusions. This provides evidence that the fracture density and aspect-ratio directly affects the parameter  $\epsilon$ . This evidences it also observed in previously work of Assad et al (1992, 1996).

Figure 3.1- P-wave seismograms as a function of change in p-wave polarization from  $0^\circ$  (x direction) to  $90^\circ$  (z direction) for sample SFC4 (isotropic).



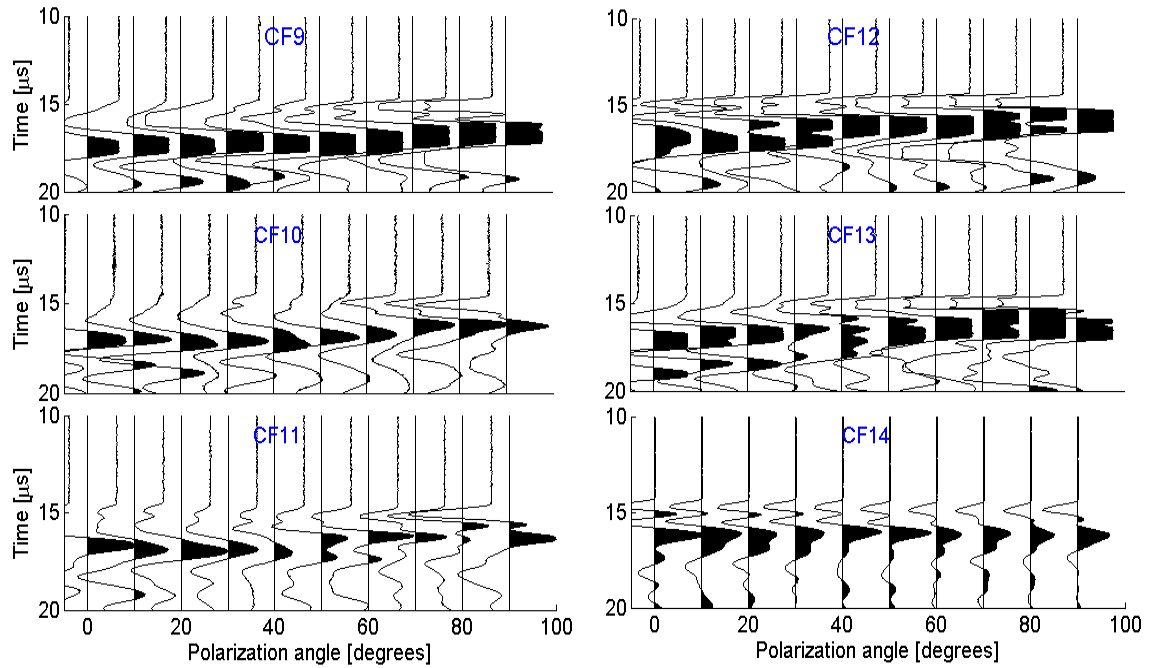
Source: From author.

Figure 3.2- Unfiltered P-waveforms as a function of change in P-wave polarization for  $0^\circ$  (x direction) to  $90^\circ$  (z direction) for all samples with crack density of 5%.



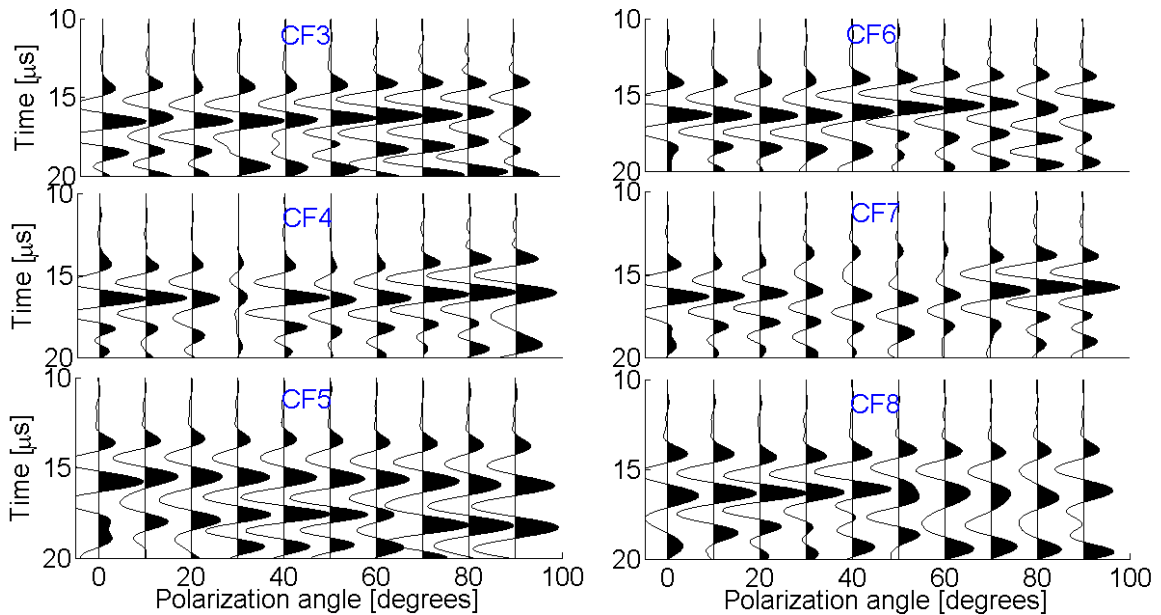
Source: From author.

Figure 3.3- Unfiltered P-waveforms as a function of change in P-wave polarization for  $0^\circ$  (x direction) to  $90^\circ$  (z direction) for all samples with crack density of 8%.



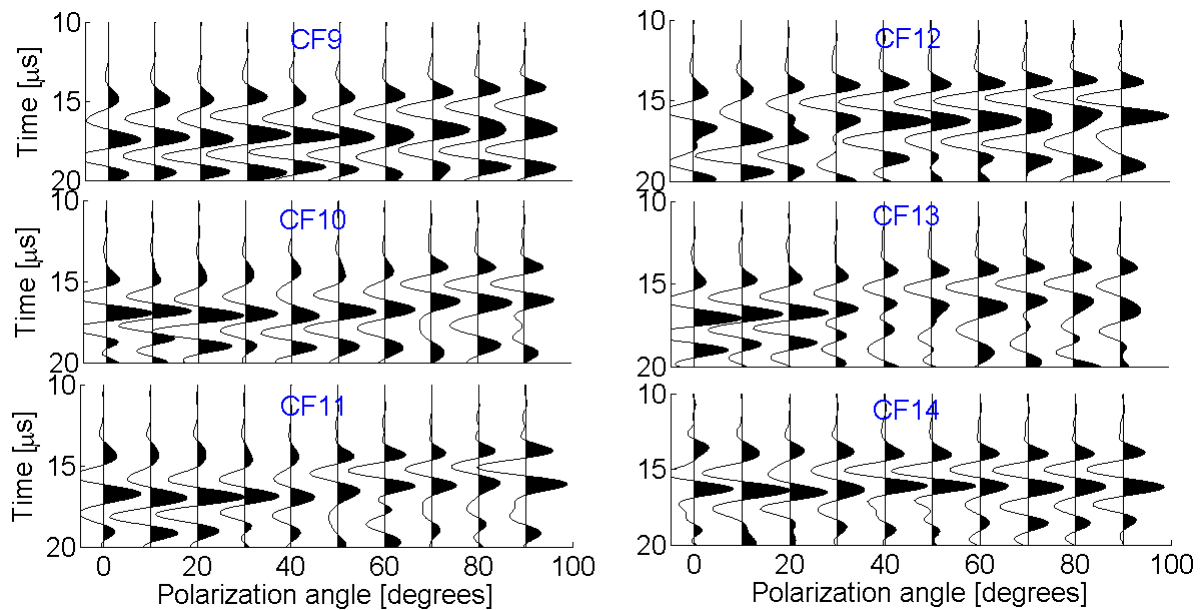
Source: From author.

Figure 3.4- Filtered P-waveforms as a function of change in P-wave polarization for  $0^\circ$  (x direction) to  $90^\circ$  (z direction) for all samples with crack density of 5%.



Source: From author.

Figure 3.5- Filtered P-waveforms as a function of change in P-wave polarization for 0° (x direction) to 90° (z direction) for all samples with crack density of 8%.



Source: From author.

Table 3.1- Compressional wave velocities (for X and Z directions) and anisotropic parameter  $\epsilon$  calculated according to equation (7).

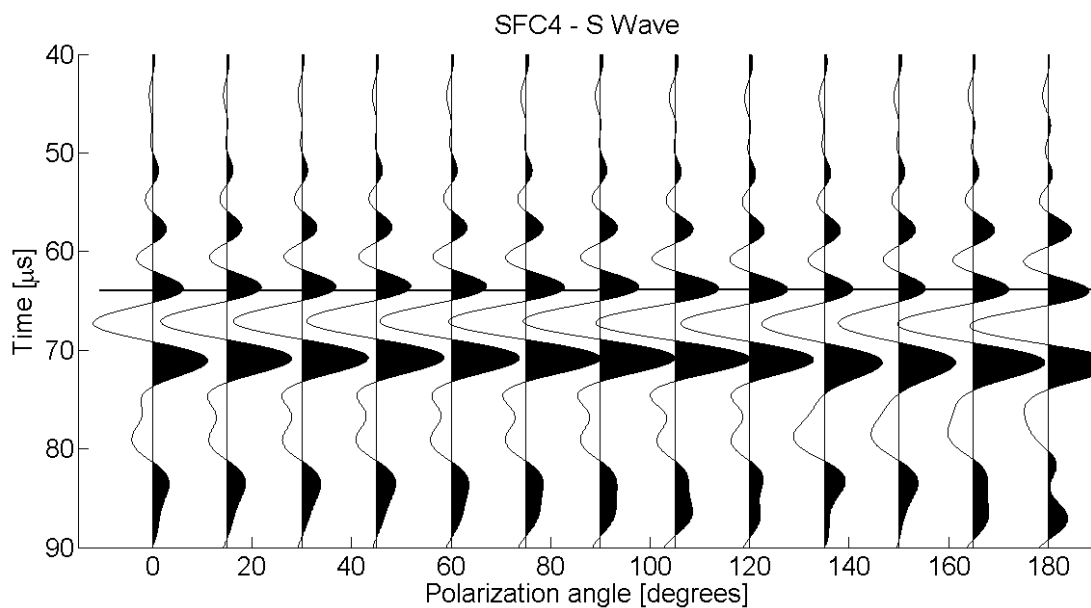
Sample Names	$V_{pz}$ (m/s)	$V_{px}$ (m/s)	$\epsilon$ (%)
SFC4	2630.2	2630.2	0
CF3	2247.12	2478.6	10.83
CF4	2378.79	2511.9	5.75
CF5	2248	2296.9	2.19
CF6	2163.6	2308.2	6.9
CF7	2207.5	2350.67	6.69
CF8	2288	2400	5.01
CF9	2144.9	2442.1	14.81
CF10	2104.05	2314.52	10.5
CF11	2226.97	2445.6	10.3
CF12	2211.5	2660.3	22.35
CF13	2089.98	2566.1	25.37
CF14	2231.6	2351.1	5.49

Source: From author.

### 3.3 Shear wave (S) velocities

In the next step in this work, the S-wave velocities from transmission through the samples were analyzed. As for the P waves, transmitted S-waveforms were measured in the cracked samples as well as in the isotropic reference model. For all recorded seismograms, the initial polarization was parallel to the X direction, denoted as  $0^\circ$ . For all S-wave seismograms the wave propagation was along to the Y direction. Figure 3.6 shows the recorded S-wave transmission seismograms for propagation in the Y direction as a function of the angle of S-wave polarization of isotropic sample. As expected, the seismograms recorded in the reference model show uniform first arrivals for all rotations of the polarization angle.

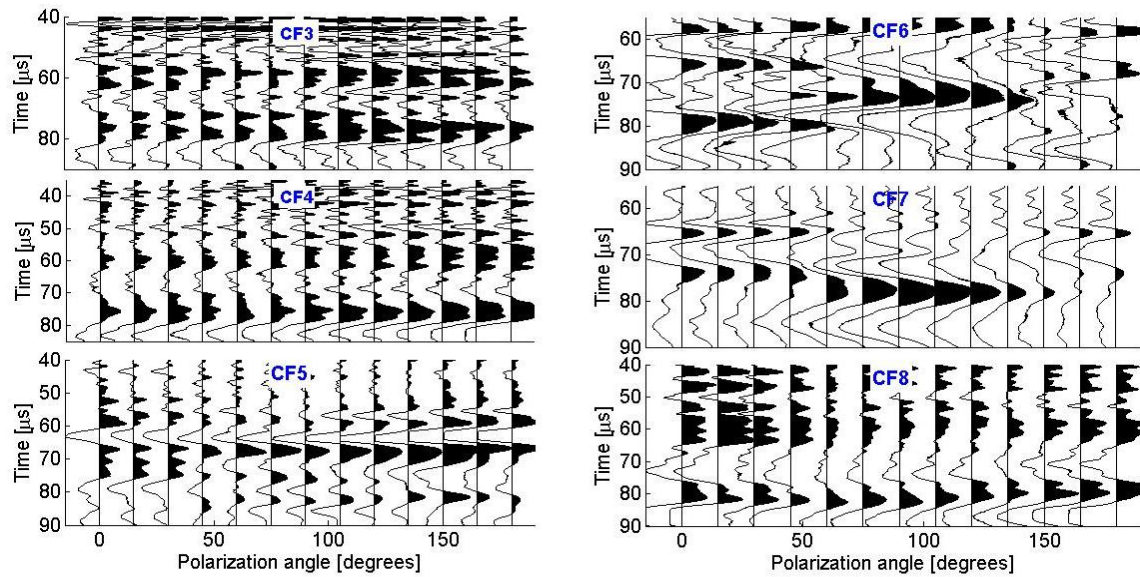
Figure 3.6- S-wave seismograms as a function of change in polarization from  $0^\circ$  to  $180^\circ$  for propagation in the Y direction in the reference sample (SFC4).



Source: From author.

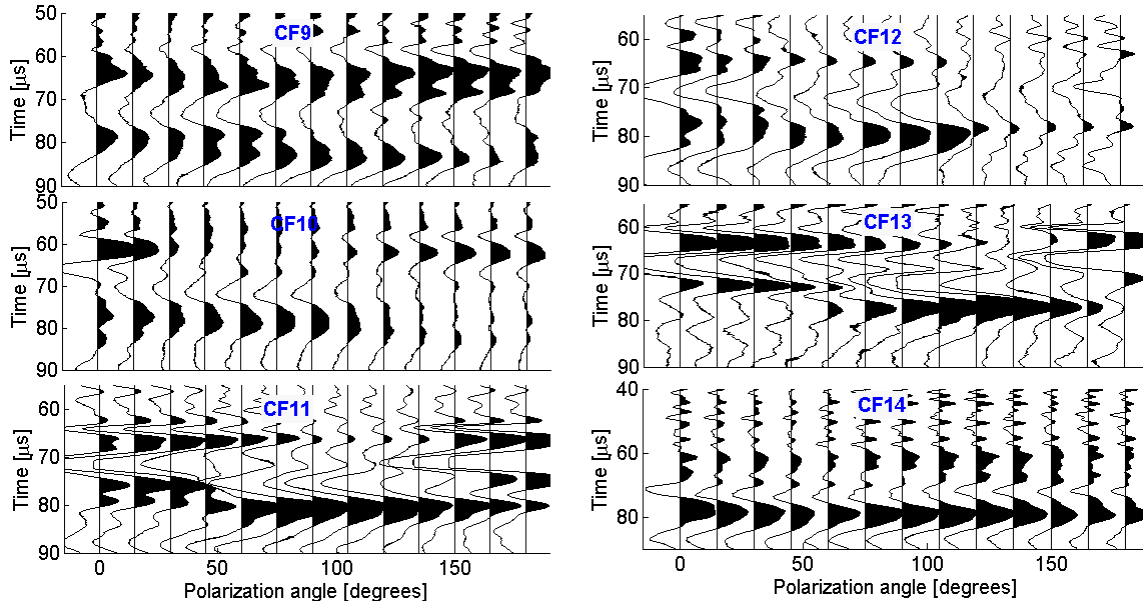
Figure 3.7 and Figure 3.8 shows the seismograms of high frequency recorded at six cracked samples with 5 % crack density and six cracked samples with 8% crack density. All the seismograms are function of polarization angle (in the plane XY) for S-wave propagation in the Y direction as recorded in the reference sample. Due the high frequency noise from environment as well as show a visible shear.

Figure 3.7- S-wave seismograms as a function of change in polarization from 0° to 180° for propagation in the Y direction in the samples with 5% crack density before filtering.



Source: From author.

Figure 3.8- S-wave seismograms as a function of change in polarization from 0° to 180° for propagation in the Y direction in the samples with 8% crack density before filtering.



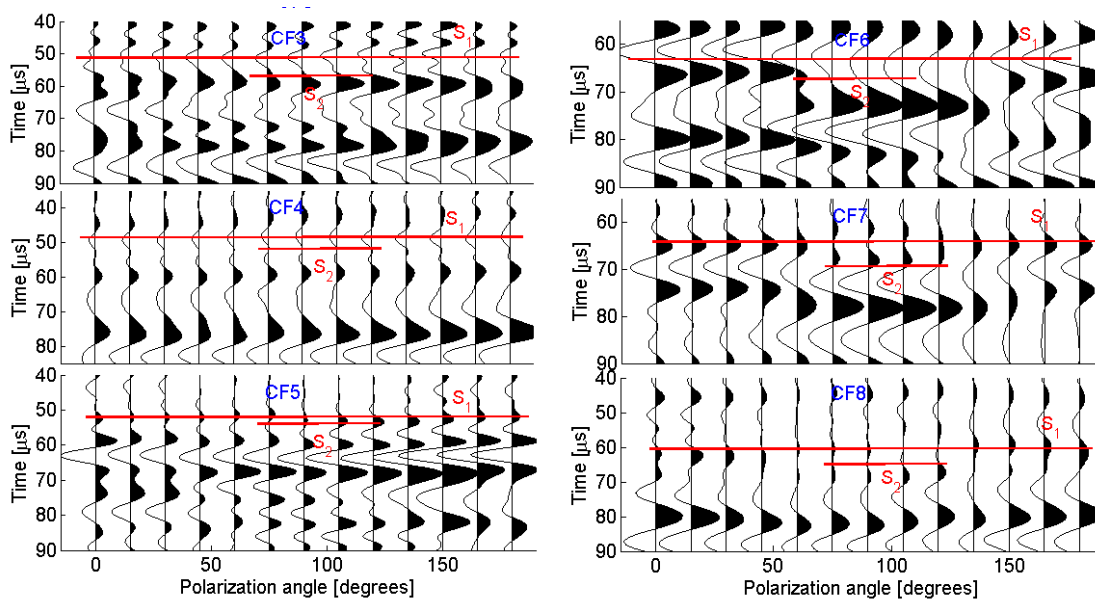
Source: From author.

For a better understanding of the two separate peaks, we applied in most samples a band-pass filter of 40–70–130–160 kHz (perfect pass between 50 and 170 kHz, when the center of filter are in 100 kHz, with linear cut-off ramps in the ranges 20–

40 kHz and 130–200 kHz) The Cut-off frequency of 160 kHz approximately coincides with the end of the first peak in Figure 3.7 and Figure 3.8. The result obtained as the difference between the original and filtered seismograms, is shown in Figure 3.9 and Figure 3.10.

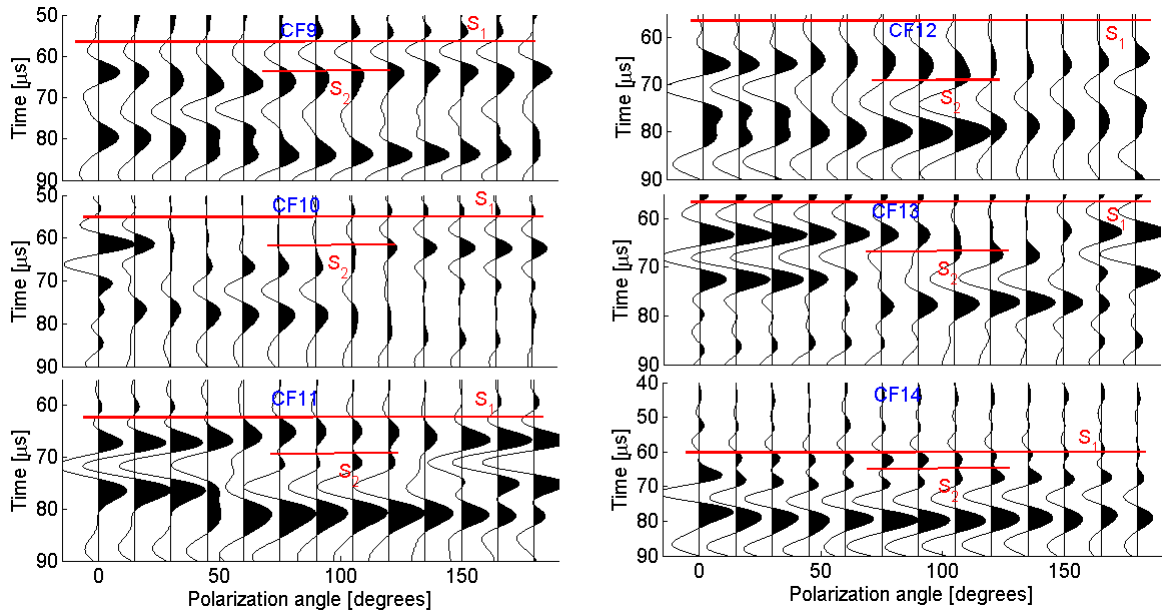
Samples with cracks show the separation of the two different S waves ( $S_1$  and  $S_2$ ) as can see in Figure 3.9 and Figure 3.10. For compute the  $V_{s1}$  and  $V_{s2}$  was necessary select the first arrival in  $0^\circ$  ( $S_1$ ) and first arrival in  $90^\circ$  ( $S_2$ ) and the dimensions of each sample (exposed in Table 2.2). The Thomsen's parameter  $\gamma$  was calculated and can be seen in Table 3.2. The errors are ranging from  $\pm 7.07$  m/s to  $\pm 13.68$  m/s.

Figure 3.9- S-wave seismograms as a function of change in polarization from  $0^\circ$  to  $180^\circ$  for propagation in the Y direction in the samples with 5% crack density after filtering and with the indicate of  $S_1$  and  $S_2$ .



Source: From author.

Figure 3.10- S-wave seismograms as a function of change in polarization from 0° to 180° for propagation in the Y direction in the samples with 8% crack density after filtering and with the indicate of S1 and S2.



Source: From author.

Table 3.2- Shear wave velocities (for Y direction) and anisotropic parameter  $\gamma$  calculated according to equation (8).

Sample Names	$V_{s1}$ (m/s)	$V_{s2}$ (m/s)	$\gamma$ (%)
SFC4	1306.6	1306.6	0
CF3	1337.13	1202.75	11.80
CF4	1322.65	1222.12	8.56
CF5	1264.17	1217.23	3.93
CF6	1196.12	1109.45	8.12
CF7	1174.5	1088.93	8.17
CF8	1244.13	1157.05	7.81
CF9	1241.23	1097.92	13.91
CF10	1258.61	1116.03	13.59
CF11	1245.09	1118.3	11.98
CF12	1291.52	1108.59	17.86
CF13	1279.56	1084.35	19.62
CF14	1252.65	1165.74	7.73

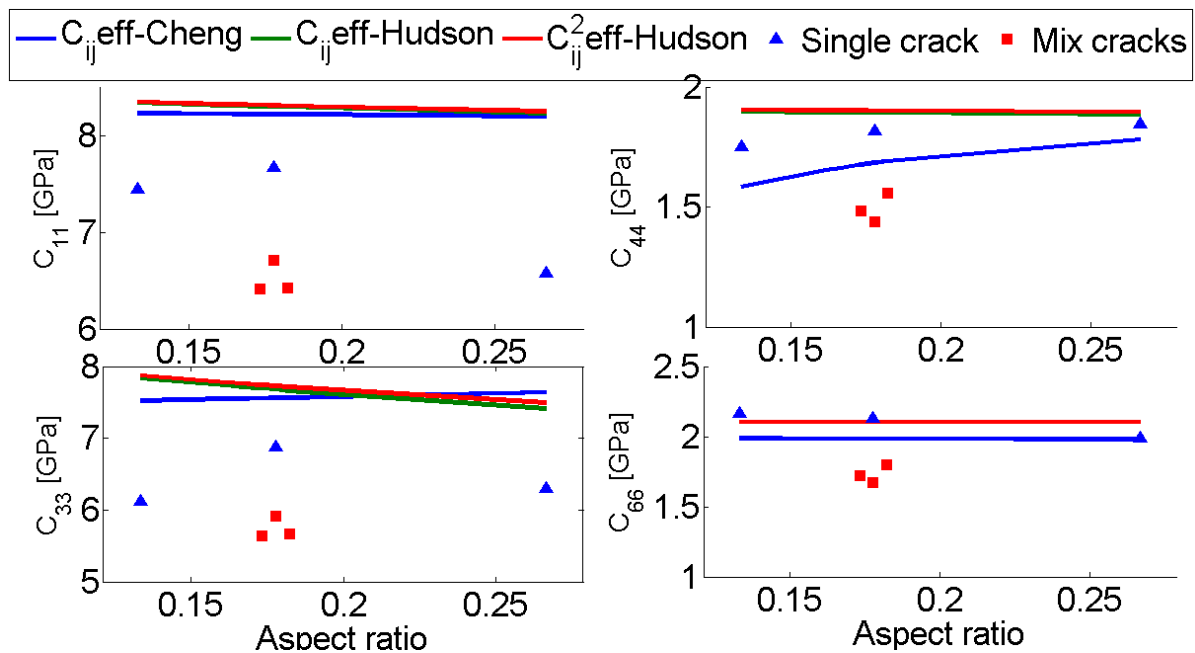
Source: From author.

### 3.4 Elastic stiffness tensor components

The description of the anisotropic medium, mathematically, is given by the constants elastics of stiffness tensor that is calculated here. For compute  $C_{11}$  and

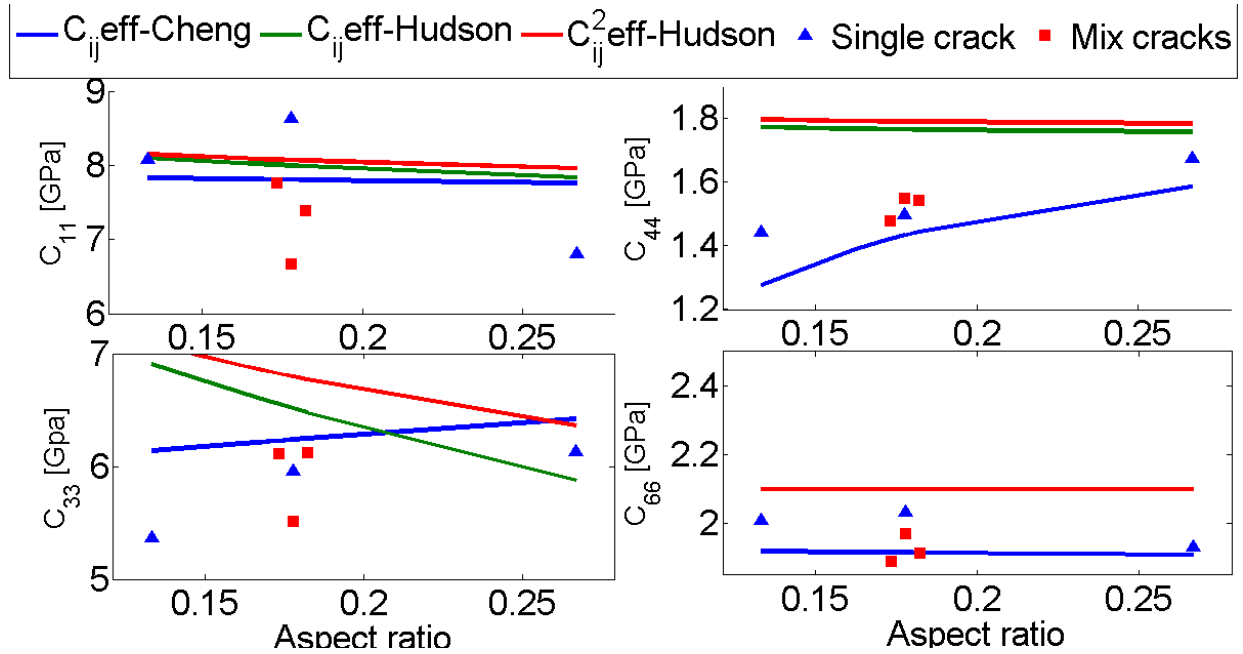
$C_{33}$  was necessary select the sample density (see Table 2.2) and the  $V_p$  in  $90^\circ$  and  $0^\circ$  (see Table 3.1) for use in the equations (3) and (4), respectively. The same way, for compute  $C_{44}$  and  $C_{66}$ , it was necessary select the sample density and the velocities  $V_{s2}$  and  $V_{s1}$  (see Table 3.2) for use in equations (5) and (6), respectively. The Figure 3.11 and Figure 3.12 shows the stiffness coefficients ( $C_{11}$ ,  $C_{33}$ ,  $C_{44}$  and  $C_{66}$ ) for both crack densities as well as the theoretical predictions performed by Hudson (1981) and Eshelby-Cheng (1993) models. It is possible in both figures that best fit between the theoretical and experimental results occurs for Eshelby-Cheng (1993). An exception is the  $C_{11}$  parameter that exhibits almost the same behavior for both predictions.

Figure 3.11- Constants of elastic stiffness tensor for 5% crack density. The green line show trends of Hudson's model with first correction, the red line trends of Hudson's model with second correction, the blue line trends of Eshelby-Cheng's model, the blue triangles are samples with single crack and red squares are mix cracks.



Source: From author.

Figure 3.12- Constants of elastic stiffness tensor for 8% crack density. The green line show trends of Hudson's model with first correction, the red line trends of Hudson's model with second correction, the blue line trends of Eshelby-Cheng's model, the blue triangles are samples with single crack and red squares are mix cracks.



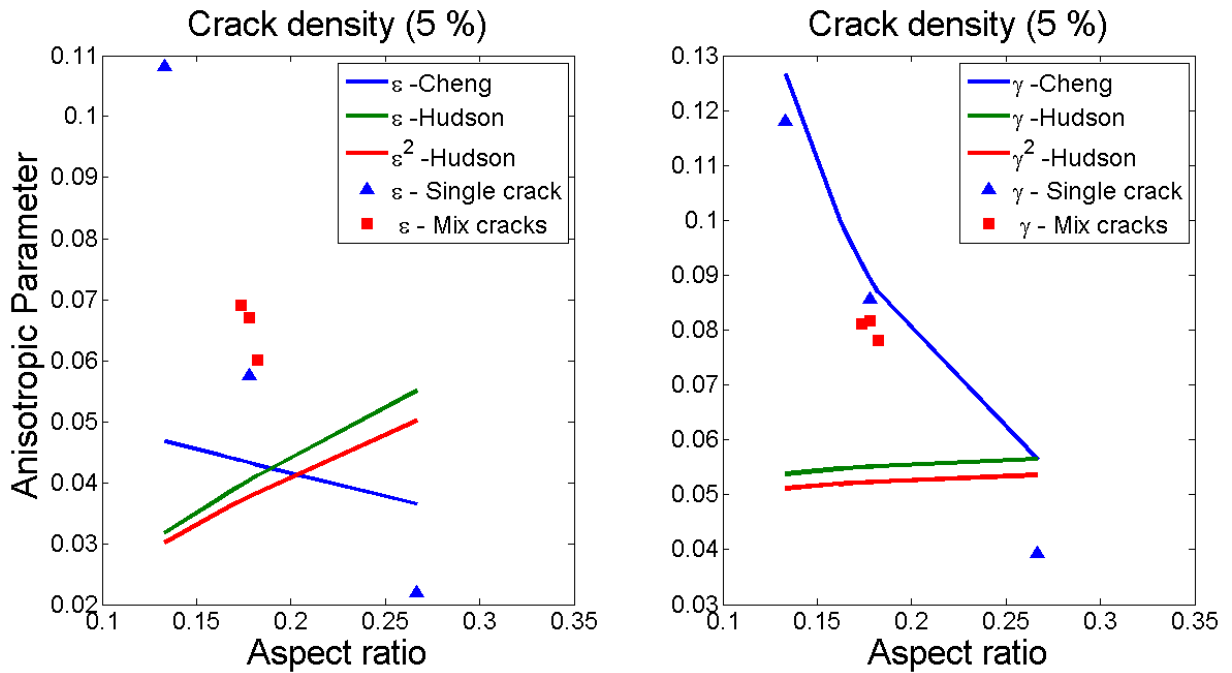
Source: From author.

### 3.5 Thomsen's parameters

Thomsen (1986) parameter  $\varepsilon$  is directly related to the ratio between  $t_{p0}$  and  $t_{p90}$  (for P-wave) which are the highest and lowest P-wave travel times observed in a fractured medium. While  $\gamma$  parameter is directly related to the ratio between  $t_{s2}$  and  $t_{s1}$  (for S-wave) which are the highest and lowest S-wave travel times in this fractured medium. For compute these parameters is necessary have the constants of elastic stiffness tensor presented earlier or they can be also calculated from the velocities. The values of  $\varepsilon$  and  $\gamma$  can be seen in Table 3.1 and Table 3.2, respectively. The Figure 3.13 and Figure 3.14 show the Thomsen's parameters calculated for each crack sample and the trends models for both densities. The predictions by the theoretical Hudson (1981) and Eshelby-Cheng (1993) models shows the opposite behaviors between them. While Hudson (1981) increases with aspect ratio, Eshelby-Cheng (1993) decreases a show a best fit with the experimental results mainly for S-wave measurements.

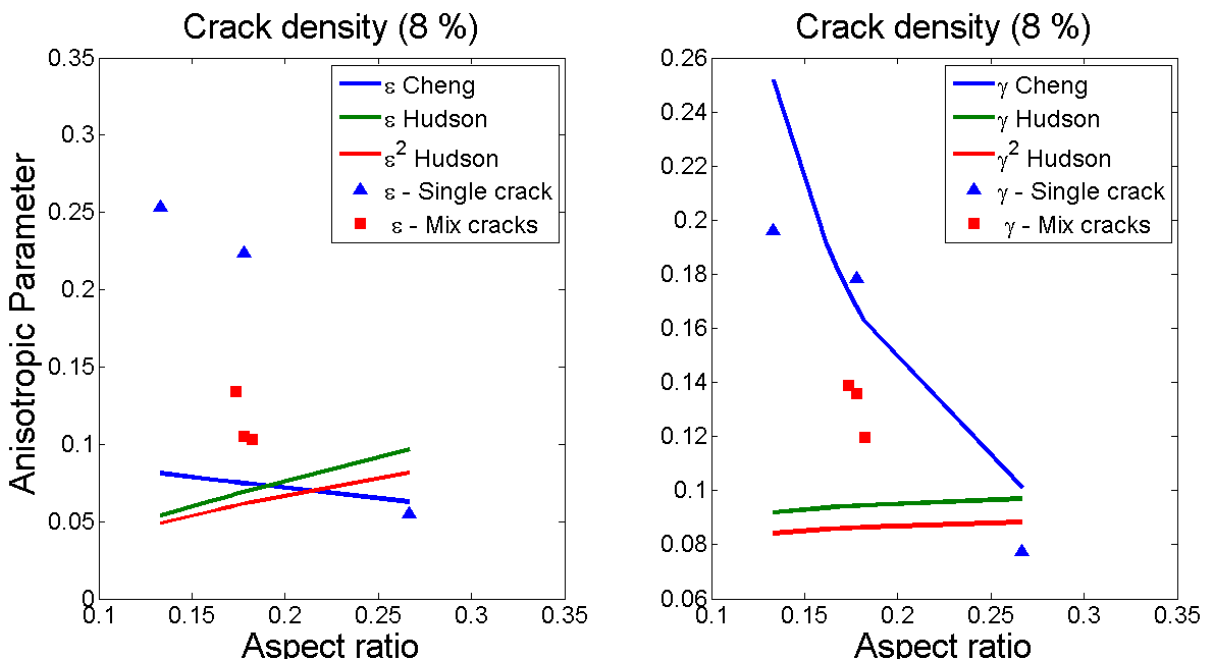
The error to estimation  $\varepsilon$  parameter is ranging from  $\pm 2.27\%$  to  $\pm 3.43\%$  and to  $\gamma$  is from 2.36% to 3.2%.

Figure 3.13- Thomsen's parameter of 5% crack density with samples and trends of Hudson (first correction in green line and second correction in red line) and Eshelby-Cheng models (in blue line).



Source: From author.

Figure 3.14- Thomsen's parameter of 8% crack density with samples and trends of Hudson (first correction in green line and second correction in red line) and Eshelby-Cheng models (in blue line).



Source: From author.

## CHAPTER 4

In this chapter the discussion will be about the results shown in previous chapter. We will comment about the considerations of comparisons among the curves of Thomsen's parameters ( $\epsilon$  and  $\gamma$ ) and the constants of the elastic stiffness tensor based on theoretical models proposed by Hudson and Eshelby-Cheng and the conclusions after analysis.

### 4.1. Discussions

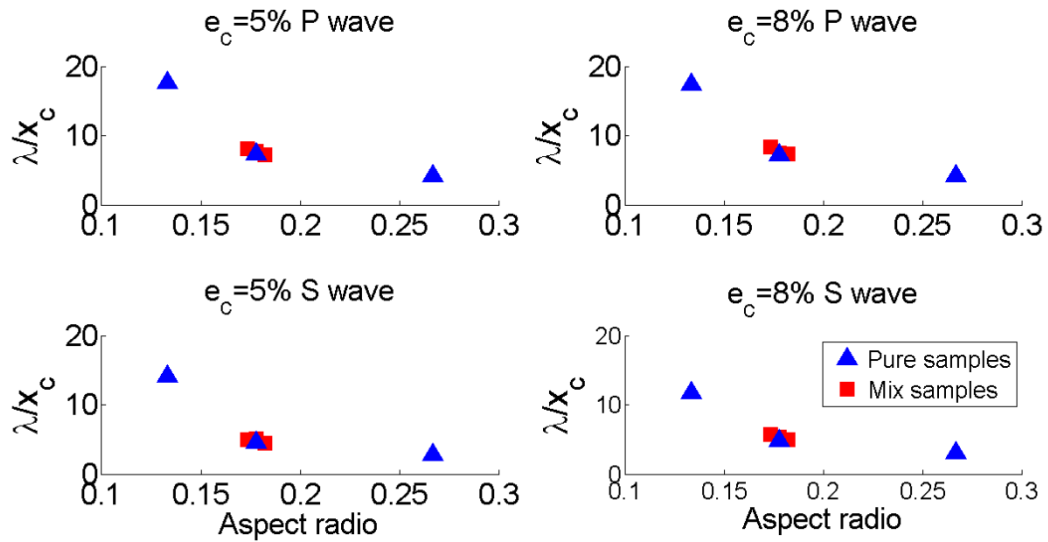
Two assumptions were investigated to ensure that the laboratory measurements are consistent with the condition of effective medium for all cracked models. The first was the wavelength ( $\lambda$ ) of source is much greater than the distance between cracks ( $x_c$ ) and the diameter of cracks ( $d_c$ ). Figure 4.1, shows the relationship between  $\lambda/x_c$  (wavelength/distance between cracks) for both P- and S-wave and densities as well. Figure 4.2 shows ratio between  $\lambda/d_c$  (wavelength/diameter of cracks) also for both waves propagation modes. Through the ratios shown in Figure 4.1 and Figure 4.2, the ratios of wavelength by distance of cracks as well as the wavelength by diameter of cracks are at least equal 2. These results can ensure the applicability of effective model assumption in this case.

It is possible to observe in Figure 3.11 and Figure 3.12 the curves of Hudson and Eshelby-Cheng's models for constants of elastic stiffness tensor have tends similar to both density, but with the difference between lies are sharpest for the 8% crack density. For Thomsen's parameters in Figure 3.13 and Figure 3.14 is possible to see for Hudson's model, independently of crack density, the  $\epsilon$  and  $\gamma$  tend to increase with aspect ratio differently of Eshelby-Cheng's model which is tend to decrease with aspect ratio. This differences are crucial to choose the best model to use for predicts trends.

To analyze all cracked samples and better understating them, will be divide the discussions of results in two groups of crack density: 5% (1° group) and 8% (2°

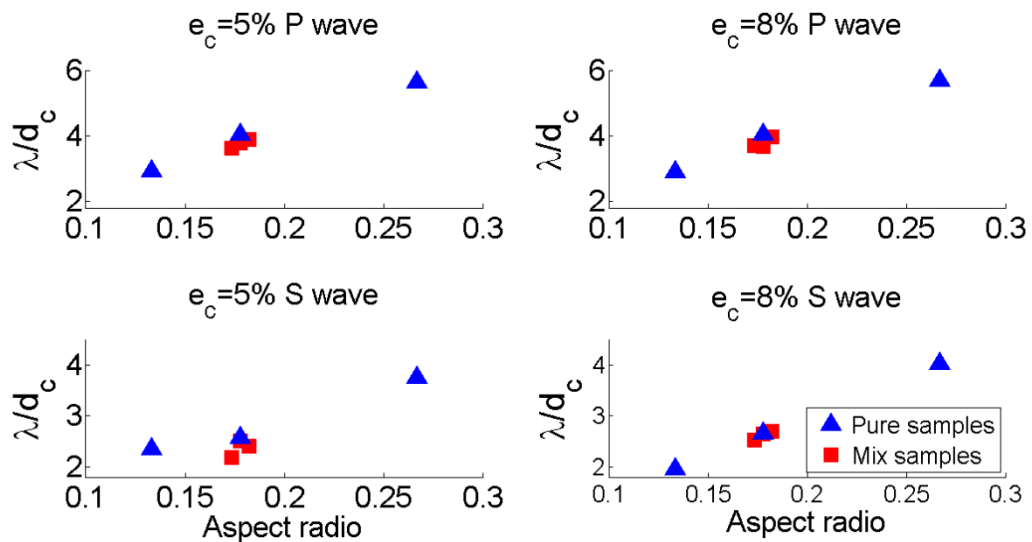
group) and these two groups have a subdivision in other two groups of crack type: single (A) and mix (B) as shown in Table 4.1.

Figure 4.1- Ratio between  $\lambda/x_c$  (wavelength/distance between cracks) for all twelve samples.



Source: From author.

Figure 4.2- Ratio between  $\lambda/d_c$  (wavelength/diameter of cracks) for all twelve samples.



Source: From author.

Table 4.1- Groups in which the samples are divided.

Samples	$e_c=5\%$ (Group 1)	$e_c=8\%$ (Group 2)
Single (A)	CF3, CF4, CF5	CF12, CF13, CF14
Mix (B)	CF6, CF7, CF8	CF9, CF10, CF11

Source: From author.

#### 4.1.1. Compressional (P) and shear (S) velocities

In this work were performed measurements of velocities with the angle between of the cracks plane and wave polarization. The velocity of compressional wave is smaller when the angle is  $0^\circ$  ( $V_{p_x}(0^\circ)$ ) and bigger when the angle is  $90^\circ$  ( $V_{p_z}(90^\circ)$ ). Already for shear wave velocities, as was cited in crack models description,  $V_{s_1}$  and  $V_{s_2}$  are separated in  $90^\circ$  and  $V_{s_1}$  is bigger than  $V_{s_2}$ .

As can see in Table 3.1 and Table 3.2 the velocities of the sample reference SFC4 (uncracked) is bigger than all other samples. This happening because when there are some obstacles in the way of wave, it tends to overcome of the obstacles. In case of samples in this work, the obstruction is the rubber cracks that have velocity smaller than the matrix of epoxy. So, the uncracked sample that no has any crack tends to have higher velocities.

In 1A Groups were noted three different behaviors. The compressional velocities ( $V_{p_x}(0^\circ)$  and  $V_{p_z}(90^\circ)$ ) and shear velocities ( $V_{s_1}$  and  $V_{s_2}$ ) are higher for CF3 sample, after for CF4 and smaller for CF5, in this case almost the same. The same behavior happens in 2A Group. The differences are higher for CF13 sample, after CF12 and smaller for CF14. These behaviors are easily explained due to aspect ratio. How small the aspect ratio samples, higher will be the difference between velocities. In 1B Group, as well as the 2B Group, is noted a homogenous behaviors, because the mix of cracks with different aspect ratio causes few changes in velocities that are related to proportion of each crack.

#### 4.1.2. Coefficients of elastic stiffness tensor

As it mentioned before, the trends of elastic coefficients are equal for both cracks densities. So the observations are the same for the Group 1 and 2. The analyses beginning with samples with single cracks, because it has just one type of crack, so give limits for the curves of parameters and coefficients with variation of aspect ratio. It is clearly that the Group A control the behavior of the coefficients and is similar, in general, with the Eshelby-Cheng's model, mostly in  $C_{44}$  coefficient. The values of Group 1B are underestimated in the both model curve and samples with single crack values. But, they are in a region that the values are near of the predicted values by Eshelby-Cheng's (1993) model.

The values Group 2B are, in general, underestimated for coefficients related with P-wave (e. g.,  $C_{11}$  and  $C_{33}$ ). However for related S-wave (e. g.,  $C_{44}$  and  $C_{66}$ ) they are close of the single sample with the aspect ratio similar of them (CF13 – see Figure 3.12) and the Eshelby-Cheng's prediction is nearly too.

#### 4.1.3. Thomsen's parameters

The analysis of Thomsen's parameters relies on the information about velocities (see Table 3.1 and Table 3.2). Therefore these parameters will be follow the behavior of velocities. In other words, the samples with higher difference between the two P- or S-wave velocities will have higher values of  $\epsilon$  and  $\gamma$ . When see the  $\epsilon$  for both crack density (see Figure 3.13 and Figure 3.14) the samples with single crack given the trends similar Eshelby-Cheng's model, although the values are overestimated when compared with the model curve. As well as  $\gamma$  the values of samples are very similar to the curve predicted by Eshelby-Cheng's.

It is valid to highlight two specific samples that are single and have smaller aspect ratio: CF5 and CF14. CF5 has smaller aspect ratio of Group 1 and CF14 of group 2. Because of the small aspect ratio ( $d_c \approx b_t$ ) the wave see cracks as spheres so

the medium looks like an isotropic homogeneous medium. Although both have similar behavior the parameters of CF14 are bigger than CF5 due to crack density.

The analyses about samples with mix cracks are different, because the variations of cracks, considering that any of models showed have a good approach for this specific case. Although, most of values of these samples are concentrated in the middle of values of samples with single crack, other method to see if the results of samples with mix cracks follow other trend, is calculate the parameters for Voigt and Reuss bounds. Voigt and Reuss can describe any isotropic effective elastic moduli based on two assumptions: 1) the volume fraction of each phase, 2) the elastic moduli of the each phase (Mavko & Mukerji, 2009). Here we use mathematical formulation of Voigt and Reuss bound to investigate the anisotropic parameters for mixed aspect –ratio cracks.

The similar Voigt bound (upper bound) for the Thomsen's parameters is given as

$$\varepsilon_V = \sum_{i=1}^3 C_{\%i} \varepsilon_i \quad (20)$$

$$\gamma_V = \sum_{i=1}^3 C_{\%i} \gamma_i \quad (21)$$

and the similar Reuss bound (lower bound) is given as

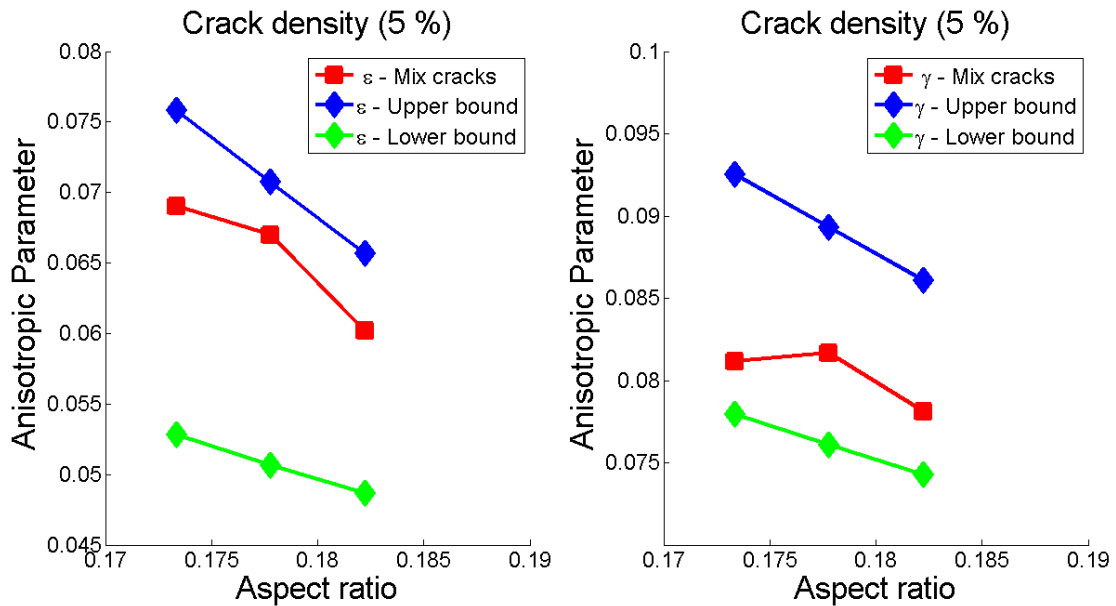
$$\varepsilon_R = \left( \sum_{i=1}^3 \frac{C_{\%i}}{\varepsilon_i} \right)^{-1} \quad (22)$$

$$\gamma_R = \left( \sum_{i=1}^3 \frac{C_{\%i}}{\gamma_i} \right)^{-1} \quad (23)$$

where the  $C_{\%i}$  is the concentration of each crack aspect ratio, the  $\varepsilon_i$  and  $\gamma_i$  are the anisotropic parameters of the single sample formed by this same crack, respectively. The samples with mix cracks and the Voigt-Reuss average for crack density 5% and 8% can see in Figure 4.3 and Figure 4.4, respectively. As it can be seen in these figures, the experimental anisotropic parameter lies on inside the Reuss and Voigt bounds from 5 % crack density. However when the crack density

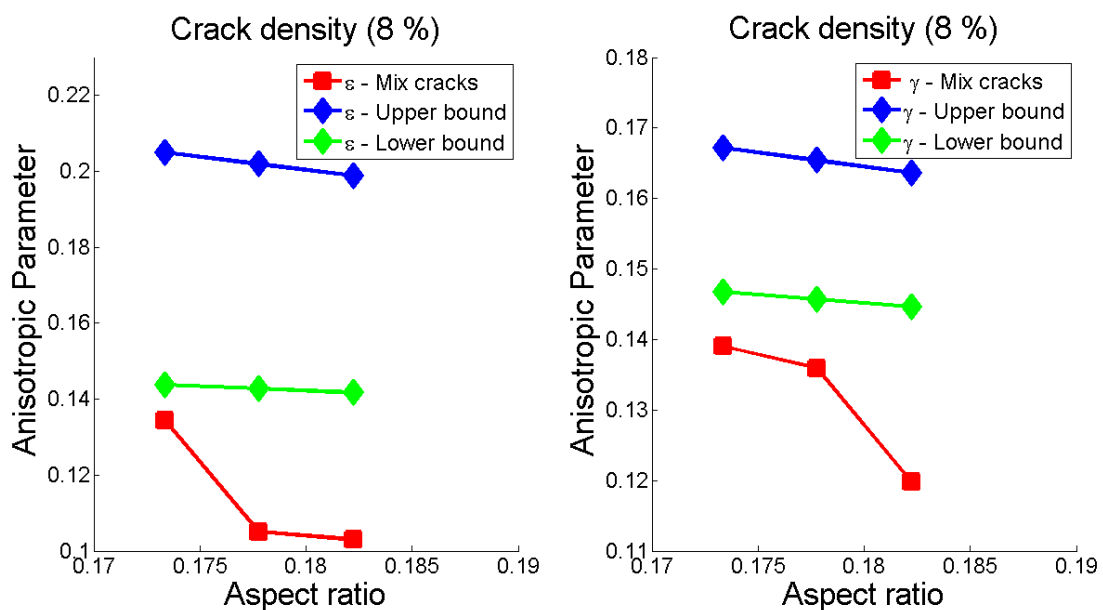
is increased for 8% the experimental values lies outside of the Reuss and Voigt bounds. This may occurred because the Reuss and Voigt bounds are used to isotropic medium. So, as longer as the crack density increase the isotropic behavior is get longer.

Figure 4.3- Thomsen's parameters for samples with mix cracks of 5% crack density with Voigt-Reuss average. The mix anisotropic values fits well between the lower (Reuss) upper (Voigt) bounds.



Source: From author.

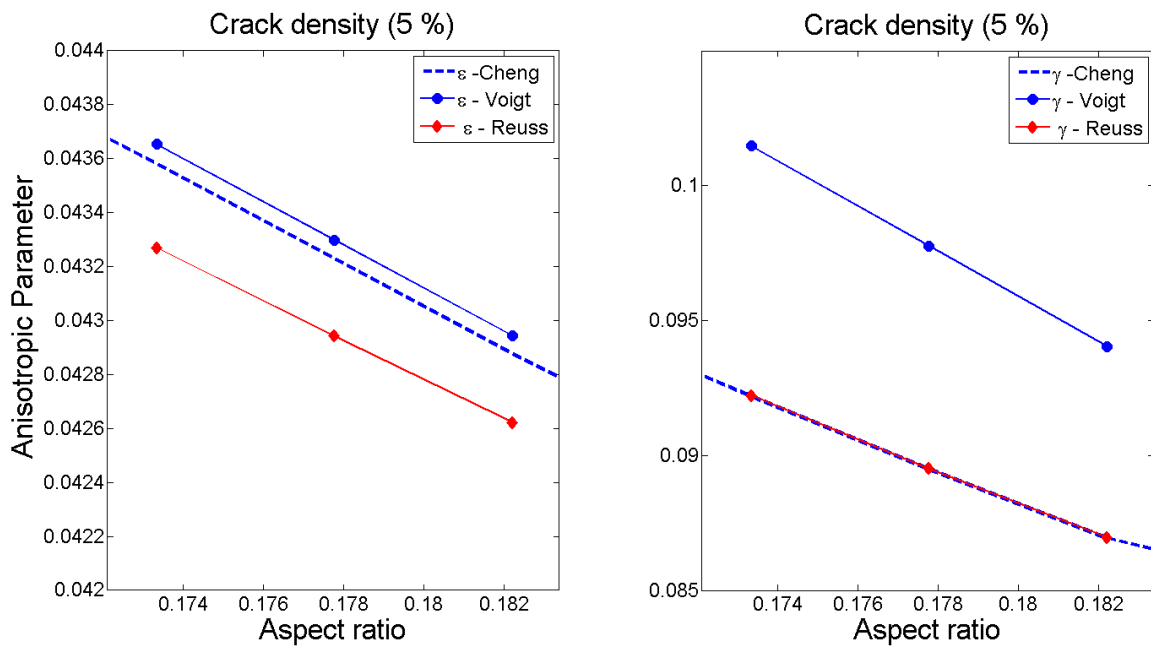
Figure 4.4- Thomsen's parameters for samples with mix cracks of 8% crack density with Voigt-Reuss average. The mix anisotropic values did not between the lower (Reuss) upper (Voigt) bounds.



Source: From author.

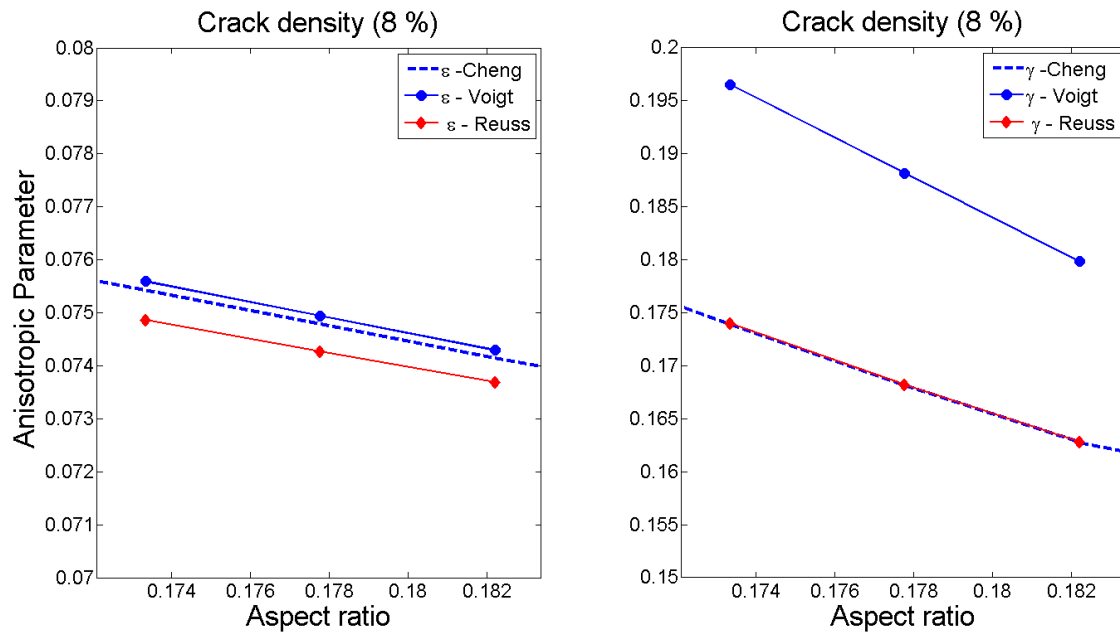
Figure 4.4 shows the values predicted by Eshelby-Cheng's (1993) model lines inside of the Reuss and Voigt bounds for both crack densities samples. It is possible to see that  $\gamma$  parameter is near to the Reuss bound (lower bound) while the  $\varepsilon$  parameter is near to the Voigt bound (upper bound). This behavior may be justified by itself formulation of these bound theories. The Reuss is harmonic mean (isostress condition) while Voigt is an arithmetic mean (isostrain condition). In this case we can infer that when P –wave propagates in the cracked medium the strain suffered by crack and solid matrix is the same and S-wave propagates the stress applied is the same.

Figure 4.5- Thomsen's parameters (predicted by Eshelby-Cheng's (1993) model) for samples with mix cracks of 5% crack density with Voigt-Reuss average. The mix anisotropic values fits well between the lower (Reuss) upper (Voigt) bounds



Source: From author.

Figure 4.6- Thomsen's parameters (predicted by Eshelby-Cheng's (1993) model) for samples with mix cracks of 8% crack density with Voigt-Reuss average. The mix anisotropic values fits well between the lower (Reuss) upper (Voigt) bounds



Source: From author.

## CHAPTER 5

### 5.1 Conclusions

In this work, we performed ultrasonic measurements through an anisotropic model built from rubber discs (penny-shaped) inclusions in an isotropic. Two groups of anisotropic models were investigated to compare the Hudson (1981) and Eshelby-Cheng's (1993) responses to the effective crack models on elastic wave propagation in anisotropic media containing aligned penny-shaped cracks. On the basis of our results, the following observations can be made:

- The elastic moduli of the shear wave ( $C_{44}$  and  $C_{66}$ ) were well predicted by Eshelby-Cheng's (1993) model for both crack densities and both types of aspect ratio types (single and mixed).
- The elastic moduli of the compressional wave ( $C_{11}$  and  $C_{33}$ ) predicted by Eshelby-Cheng's (1993) model for both crack densities shown an underestimation related to the experimental values obtained for both crack densities and both types of aspect ratio types (single and mixed).
- The decrease in anisotropic parameter  $\gamma$  was observed both for experimental and Eshelby-Cheng's (1993) model prediction (for both crack densities) as the aspect model ratio increased. This behavior was contrary to that one exhibited by the Hudson's (1981) model. The best fit between the experimental and theoretical prediction occurred by the Eshelby-Cheng's (1993) model.
- The decrease in anisotropic parameter  $\varepsilon$  was observed both for experimental and Eshelby-Cheng's (1993) model prediction (for both crack densities) as the aspect model ratio increased. This behavior was contrary also, to that one exhibited by the Hudson's (1981) model. For both models did not occur a good fit between the models and experimental results.
- For samples with mixed crack aspect ratio the theoretical prediction was better performed by the Eshelby-Cheng's (1993) model for shear wave case only and sample of Group 1B (crack density of 5%). This prediction was also lies in the Voigt-Reuss bounds. The Voigt-Reuss bounds is

generally used for isotropic medium, so when the medium tend to be a low crack density medium (Group 1B) values are in general, between the bounds. When the crack density increases, the values of parameters are out of bounds.

## REFERENCES

- ASSAD, J. et al. Elastic wave propagation in a medium containing oriented inclusions with a changing aspect ratio: a physical model study. *Geophys. d. Int.*, v. 125, p. 163-172, 1996.
- ASSAD, J. M; TATHAM, R. H; MCDONALD, J. A. A physical model study of microcrack-induced anisotropy. *Geophysics*, v. 57, p. 1562-1570, 1992.
- CHENG, C. H. Crack models for a transversely anisotropic medium. *J. Geophys. Res.*, v. 98, p. 675–684, 1993.
- COATES, R. T; SCHOENBERG M. Finite-difference modeling of faults and fractures. *Geophysics*, v. 60, p.1514–1526, 1995.
- FIGUEIREDO, J. J. S. et al. Estimating fracture orientation from elastic-wave propagation. *Journal of geophysical research*, v. 117, p. 1-13, 2012.
- FIGUEIREDO, J. J. S. et al. Shear wave anisotropy from aligned inclusions: ultrasonic frequency dependence of velocity and attenuation. *Geophys. J. Int.*, v. 193, p. 475–488, 2013.
- ESHELBY, J. D. The determination of the elastic field of an ellipsoidal inclusion, and related problems. *Proc. Royal Soc. London A*, v. 241, p. 376–396, 1957.
- HUDSON, J. A. Wave speeds and attenuation of elastic waves in material containing cracks. *Geophys. J. R. Astron. Soc.*, v. 64, p. 133-150, 1981.
- HUDSON, J. A.; LIU, E. Effective elastic properties of heavily faulted structures. *Geophysics*, v. 64, n. 2, p.479-489, 1999.
- MAVKO, G.; MUKERJI, T. A; DVORKIN, J. *The rock physics handbook - tools for seismic analysis of porous media*. Second. ed. New York: Cambridge University Press, 2009.
- NELSON, R. A. *Geologic analysis of naturally fractured reservoirs*. second edition. [S.I.]: Elsevier, 2001.
- RATHORE, J. S; FJAER,. E; HOLT,. R. M.; RENLIE,. L. P- and S- wave anisotropy of a synthetic sandstone with controlled crack geometry. *Geophys. Prospect.*, v. 43, p. 711–728, 1995.
- SAENGER, E. H.; SHAPIRO, S. A. Effective velocities in fractured media: a numerical study using the rotated staggered finite-difference grid. *Geophysical Prospecting*, v. 50, p.183–194., 2002.

SANTOS, L. K. et al On the source-frequency dependence of fracture-orientation estimates from shear-wave transmission experiments,. *Journal of Applied Geophysics*, v. 114, p.81-100, 2015.

SAYERS, C. M. Introduction to special section: Fractures. *The Leading Edge*, v. 26, p. 1102–1105, 2007.

SHAW, R. P. Understanding the micro to macro behaviour of rock-fluid systems. *The Geological Society of London*, 2005.

THOMSEN, L. Weak elastic anisotropy. *Geophys.*, v. 51, p. 1954–1966, 1986.

WILD, P. Practical applications of seismic anisotropy. *First Break*, v. 29, p.117–124, 2011.

## **APPENDICES**

## APPENDIX A

### APPENDIX A.1- EFFECTIVE MODULI BY HUDSON

The effective moduli  $C^{eff}_{ij}$  for Hudson (1981) cracked model are given as

$$C^{eff}_{ij} = C^0_{ij} + C^1_{ij} + C^2_{ij} ,$$

$$C^0_{11} = C^0_{33} = \lambda + 2\mu ,$$

$$C^0_{13} = \lambda ,$$

$$C^0_{44} = C^0_{66} = \mu .$$

where  $\lambda$  and  $\mu$  are the Lamé parameters and  $C^1_{ij}$  and  $C^2_{ij}$  are the first and second correction due of inclusions.

The first corrections ( $C^1_{ij}$ ) are:

$$C^1_{11} = -\frac{\lambda^2}{\mu} \epsilon U_3 ,$$

$$C^1_{13} = -\frac{(\lambda + 2\mu)^2}{\mu} \epsilon U_3 ,$$

$$C^1_{33} = -\frac{(\lambda + 2\mu)^2}{\mu} \epsilon U_3 ,$$

$$C^1_{44} = \mu \epsilon U_1 ,$$

$$C^1_{66} = 0 .$$

While the second ( $C^2_{ij}$ ) corrections are represent by:

$$C^2_{11} = \frac{q}{15} \frac{\lambda^2}{\lambda + 2\mu} (\epsilon U_3)^2 ,$$

$$C^2_{13} = \frac{q}{15} \lambda (\epsilon U_3)^2 ,$$

$$C^2_{33} = \frac{q}{15} (\lambda + 2\mu) (\epsilon U_3)^2 ,$$

$$C^2_{44} = \frac{2}{15} \frac{\mu(3\lambda + 8\mu)}{\lambda + 2\mu} (\epsilon U_1)^2 ,$$

$$C^2_{66} = 0 ,$$

where  $q = 15 \frac{\lambda^2}{\mu^2} + 15 \frac{\lambda}{\mu} + 28$ , and  $\epsilon$  is the crack density ( $\epsilon = \frac{3\phi}{4\pi\alpha}$ ) and  $\alpha$  is the aspect ratio.

The parameters  $U_1$  and  $U_3$  depend on the type of inclusion:

- For inclusions with fluid:

$$U_3 = 0$$

$$U_1 = \frac{16(\lambda+2\mu)}{3(\lambda+2\mu)}$$

- For dry inclusions:

$$U_3 = \frac{4(\lambda+2\mu)}{3(\lambda+2\mu)}$$

$$U_1 = \frac{16(\lambda+2\mu)}{3(3\lambda+4\mu)}$$

- For “weak” inclusions:

$$U_3 = \frac{4(\lambda+2\mu)}{3(\lambda+2\mu)} \frac{1}{(1+K)}$$

$$U_1 = \frac{16(\lambda+2\mu)}{3(3\lambda+4\mu)}$$

with:

$$K = \frac{\kappa_f(\lambda+2\mu)}{\pi\alpha\mu(\lambda+2\mu)}$$

In this work were used the  $U_3$  and  $U_1$  for weak inclusion.

## APPENDIX A.2 - EFFECTIVE MODULI BY CHENG

The effective moduli  $C^{eff}$  for a rock containing fluid-filled ellipsoidal cracks are given as

$$C^{eff}_{ij} = C^0_{ij} - \Phi C^1_{ij}$$

where  $\Phi$  is the porosity. The first corrections  $C^1_{ij}$  are

$$C_{11} = \lambda(S_{31} - S_{33} + 1) + \frac{2\mu(S_{33}S_{11} - S_{31}S_{13} - (S_{33} + S_{11} - 2C - 1) + C(S_{31} + S_{13} - S_{11} - S_{33}))}{D(S_{12} - S_{11} + 1)}$$

$$C_{33} = \frac{(\lambda + 2\mu)(-S_{12} - S_{11} + 1) + 2\lambda S_{13} + 4\mu C}{D}$$

$$C_{13} = \frac{(\lambda + 2\mu)(S_{13} + S_{31}) - 4\mu C + \lambda(S_{13} - S_{12} - S_{11} - S_{33} + 2)}{2D}$$

$$C_{44} = \frac{\mu}{1 - 2S_{1313}}$$

$$C_{66} = \frac{\mu}{1 - 2S_{1212}}$$

with,

$$D = S_{33} S_{11} + S_{33} S_{12} - 2 S_{31} S_{13} - (S_{11} + S_{12} + S_{33} - 1 - 3C) - C(S_{11} + S_{12} + 2(S_{33} - S_{13} - S_{31}))$$

$$S_{11} = QI_{aa} + RI_a$$

$$S_{33} = Q \frac{4\pi}{3} - Q2I_{ac}\alpha^2 + Cr$$

$$S_{12} = QI_{ab} - RI_a$$

$$S_{13} = QI_{ac}\alpha^2 - RI_a$$

$$S_{31} = QI_{ac} - RI_c$$

$$S_{1313} = \frac{Q(1 + \alpha^2 I_{ac})}{2} + \frac{R(I_a + I_c)}{2}$$

$$I_a = \frac{2\pi\alpha(\cos\alpha^{-1} - \alpha S_a)}{S_a^3}$$

$$I_c = 4\pi - 2I_a$$

$$I_{ac} = \frac{I_c - I_a}{3S_a^2}$$

$$I_{aa} = \pi - \frac{3I_{aa}}{4}$$

$$I_{aa} = \frac{I_{aa}}{3}$$

$$\sigma = \frac{3\kappa - 2\mu}{6\kappa + 2\mu}$$

$$S_a = \sqrt{1 - \alpha^2}$$

$$R = \frac{1 - 2\sigma}{8\pi(1 - \sigma)}$$

where  $\alpha$  = aspect ratio = h/d,  $\kappa$  = bulk modulus of sample,  $\kappa_f$  = bulk modulus of fluid and

$$\lambda + 2\mu = \rho V_p^2,$$

$$\mu = \rho V_s^2,$$

$$\lambda = \rho (V_p^2 - 2V_s^2),$$

are Lamé parameters.